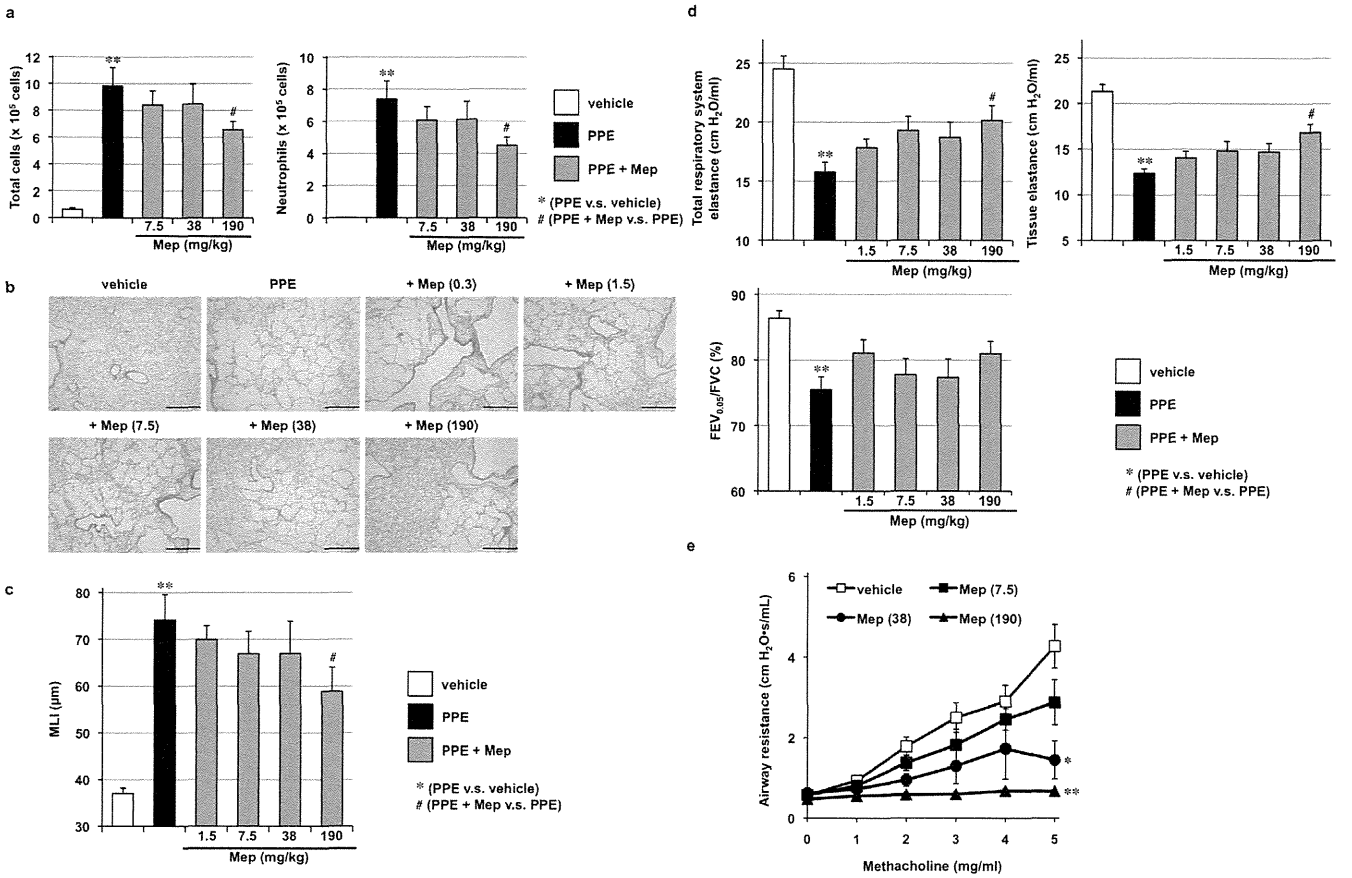

Figure 2 | Effect of oral administration of mepenzolate on PPE-induced pulmonary damage and methacholine-induced airway constriction. Administration of PPE, mepenzolate and methacholine was performed as described in the legend of Fig. 1, except that mepenzolate was administered orally (a–e). Analysis of inflammatory responses (a), histopathological examination (scale bar, 500 μm) (b), determination of the MLI (c), measurement of lung mechanics and respiratory function (d) and measurement of airway resistance (e) were carried out as described in the legend of Fig. 1. Values represent mean ± S.E.M. (n = 3–8). * or # $P < 0.05$; ** $P < 0.01$.

increase in the total number of leucocytes and the individual number of macrophages in BALF by intravenous administration of mepenzolate (10 or 100 μg/kg) was not statistically significant (Fig. 6).

Effect of different administration routes of mepenzolate on the appearance of adverse effects. To determine the appropriate administration route of any drug, it is important to consider not only its beneficial but also its adverse side-effects. For the clinical application of mepenzolate to treat COPD patients, both constipation and arrhythmia (heart palpitations) have been noted as adverse side-effects that occur due to the inhibitory effects of this drug on the muscarinic receptor and the resulting inhibition of intestinal motility and increased heart rate[22,23]. We therefore examined the effect of different routes of mepenzolate administration on defecation and heart rate in treated mice.

Mice were subjected to restraint stress as a means to increase fecal pellet output. As shown in Fig. 7, mepenzolate administration suppressed fecal pellet output with respect to control (untreated) mice for each of the routes tested. Compared to the protective effects exerted by mepenzolate against PPE-induced pulmonary damage (Fig. 1), doses administered via the intratracheal administration route that were more than 100 times higher were required to affect fecal pellet output (Fig. 7a). In contrast, less than one hundredth the dose of mepenzolate required to provide a protective effect against lung damage significantly affected fecal pellet output when the oral administration route was used (Fig. 7b). As for the intravenous or intrarectal routes of administration, roughly similar doses of mepenzolate were required for both inhibition of fecal pellet output and protection against PPE-induced pulmonary damage (Figs. 3c, 5c, 7c and 7d). These results suggest that intratracheally administered mepenzolate could protect against PPE-induced pulmonary damage without affecting gut motility. Moreover, the results also suggest that orally administered mepenzolate affects gut motility directly (but not after absorption), because the dose required to suppress fecal pellet output was much lower compared to that required for other pharmacological effects.

Lastly, we examined the effect of mepenzolate on heart rate as measured by infrared sensor. As shown in Fig. 8a, intratracheally administered mepenzolate increased heart rate only at a dose that was much higher than that required to protect against PPE-induced pulmonary damage (Fig. 1c). On the other hand, the oral, intravenous or intrarectal routes of mepenzolate administration increased the heart rate at doses roughly similar to that required for pulmonary protection (Figs. 2c, 3c, 5c, 8b–d). These results suggest that intratracheally administered mepenzolate protects against PPE-induced pulmonary damage without affecting heart rate.

Discussion

Since COPD is characterized by airflow limitation and abnormal inflammatory responses, a combination of anti-inflammatory drugs (such as steroids) and bronchodilators is the standard treatment regime[24,25]. Since mepenzolate has both anti-inflammatory and bronchodilatory activities, this drug may be beneficial for treating COPD without the concomitant use of other drugs. In particular, the anti-inflammatory effect of mepenzolate is an important property of this drug, because the inflammation associated with COPD tends to

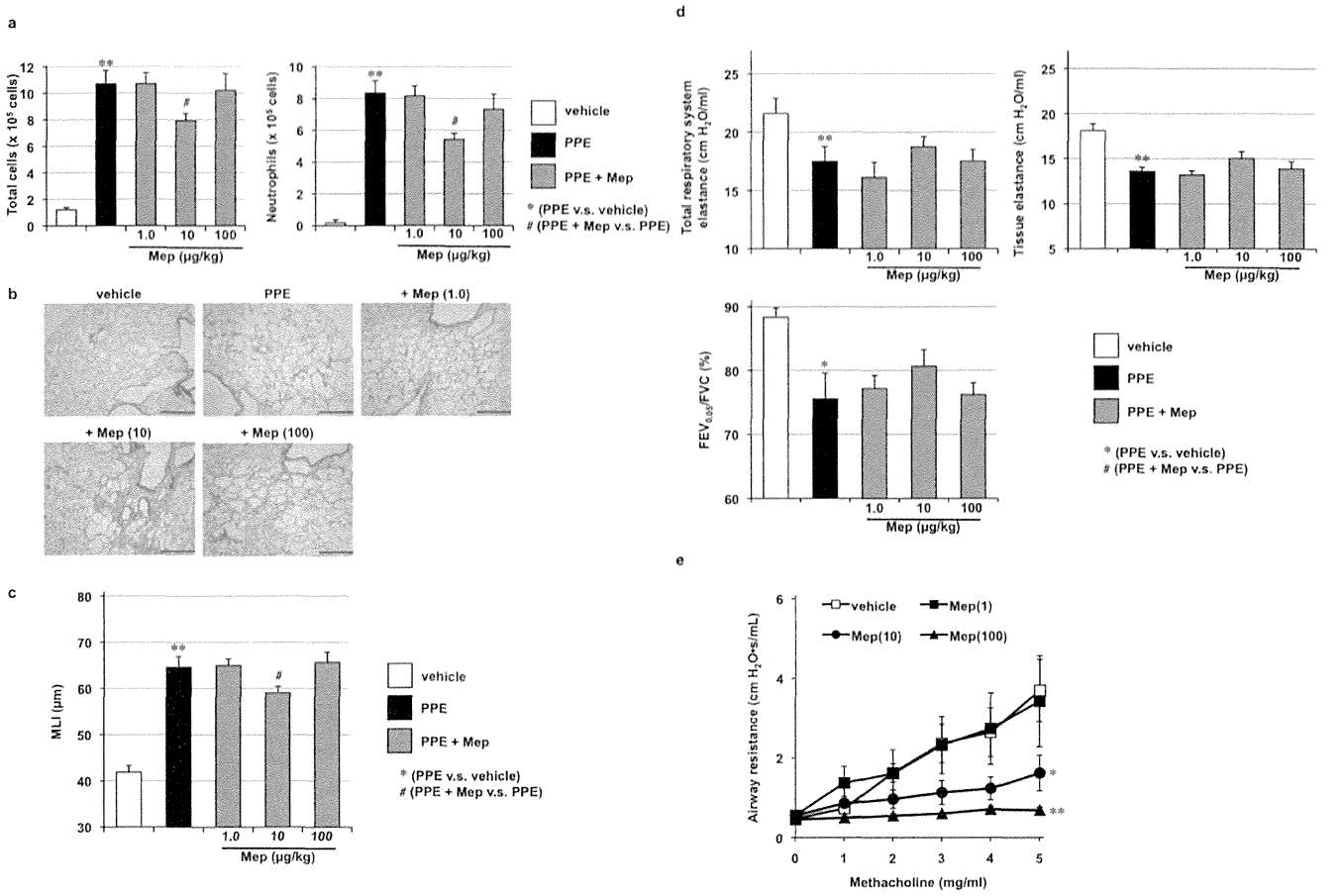

Figure 3 | Effect of intravenous administration of mepenzolate on PPE-induced pulmonary damage and methacholine-induced airway constriction. Administration of PPE, mepenzolate and methacholine was performed as described in the legend of Fig. 1, except that mepenzolate was administered intravenously (a–e). Analysis of inflammatory responses (a), histopathological examination (scale bar, 500 μm) (b), determination of the MLI (c), measurement of lung mechanics and respiratory function (d) and measurement of airway resistance (e) were carried out as described in the legend of Fig. 1. Values represent mean ± S.E.M. (n = 3–14). * or # $P < 0.05$; ** $P < 0.01$.

show resistance to steroid treatment; common steroids as such do not significantly modulate disease progression and mortality[5–7]. This insensitivity to steroids can be explained by the notion that steroids suppress the expression of pro-inflammatory genes via their action on histone deacetylase (HDAC) 2[26,27]. CS also inhibits the activity and expression of HDAC2[26]. On the other hand, mepenzolate can restore HDAC activity under inflammatory conditions[9], which may explain its superior anti-inflammatory activity to steroids under these conditions (see below). In an animal model of elastase-induced lung inflammation and emphysema, we reported that steroids do not provide protective or therapeutic benefits against PPE-induced pulmonary emphysema, alterations of lung mechanics, or respiratory dysfunction[19], whereas mepenzolate was effective against these disorders under the same experimental conditions[9]. Based on these results, we considered that mepenzolate could be therapeutically beneficial to treat COPD patients, which motivated us to examine here the effect of different routes of mepenzolate administration (intratracheal, oral, intravenous or intrarectal) on its beneficial effects (protection against PPE-induced pulmonary damage and bronchodilation) and adverse side-effects (alteration of gut motility and heart rate) in mice.

Intratracheally administered mepenzolate protected against PPE-induced pulmonary damage (inflammatory responses, pulmonary emphysema, alteration of lung mechanics and respiratory dysfunction) at a dose of 38 μg/kg and showed bronchodilation activity at a dose of 0.3 μg/kg, as reported recently[9]. We here found that this mode of administration required a much higher dose (4.7 mg/kg) to affect fecal pellet output and heart rate, thus demonstrating that intratracheally administered mepenzolate could suppress PPE-induced pulmonary damage and improve airflow limitation without affecting these other parameters, which is of particular clinical significance in terms of the use of this drug to treat COPD patients. This may be due to the fact that intratracheally administered mepenzolate is localized within the lung, in contrast to the other routes of administration studied. Furthermore, the lower dose of mepenzolate required for bronchodilation (compared to protection against PPE-induced pulmonary damage) suggests that intratracheally administered mepenzolate is localized within the bronchi rather than the alveoli, because such differences in dosage were not observed for the other forms of systemic administration.

We found here that the oral and intravenous routes of mepenzolate administration also protected against PPE-induced pulmonary damage and showed bronchodilatory activity. However, the improvement of respiratory function ($FEV_{0.05}$/FVC) by mepenzolate was not statistically significant when the drug was administered via these routes. Compared to intravenous or intratracheal administration, much higher doses of mepenzolate were required to protect against PPE-induced pulmonary damage for the oral route of administration, suggesting that the efficiency of absorption into the circulation is very poor for administration via this route. It should be noted that mepenzolate achieved beneficial and adverse effects at roughly similar doses when administered orally or intravenously (except for the effect of orally administered mepenzolate on fecal pellet output). When the route of administration was intrarectal rather than oral,

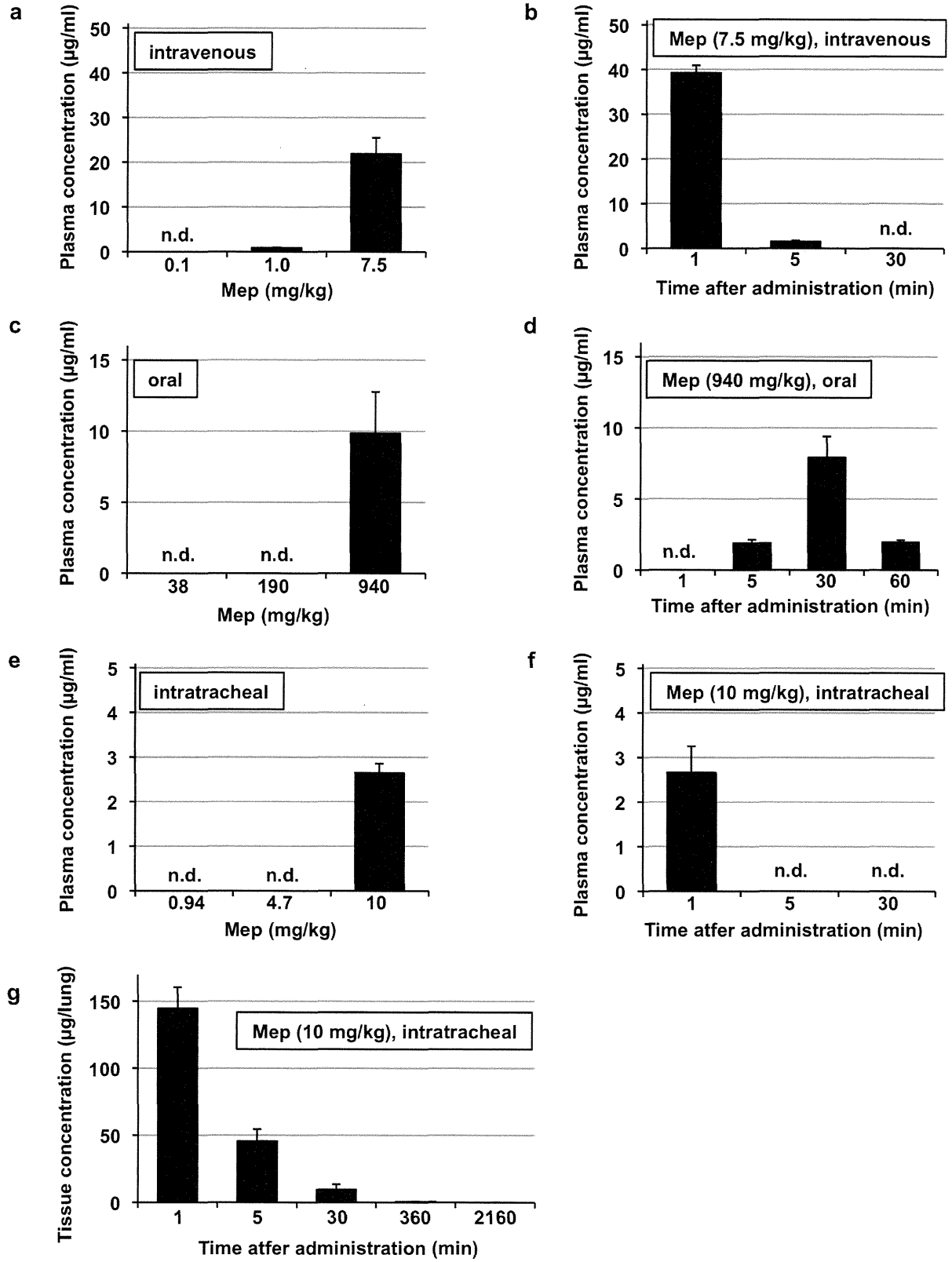

Figure 4 | Determination of the level of mepenzolate after administration through various routes. Mice were administered indicated doses of mepenzolate intravenously (a, b), orally (c, d) or intratracheally (e–g). After indicated periods (b, d, f, g), 1 min (a, e) or 30 min (c), blood samples (a–f) or lung homogenates (g) were prepared and the level of mepenzolate was determined as described in the Materials and Methods. Values are mean ± S.E.M. (n = 3–4). n.d., not detected.

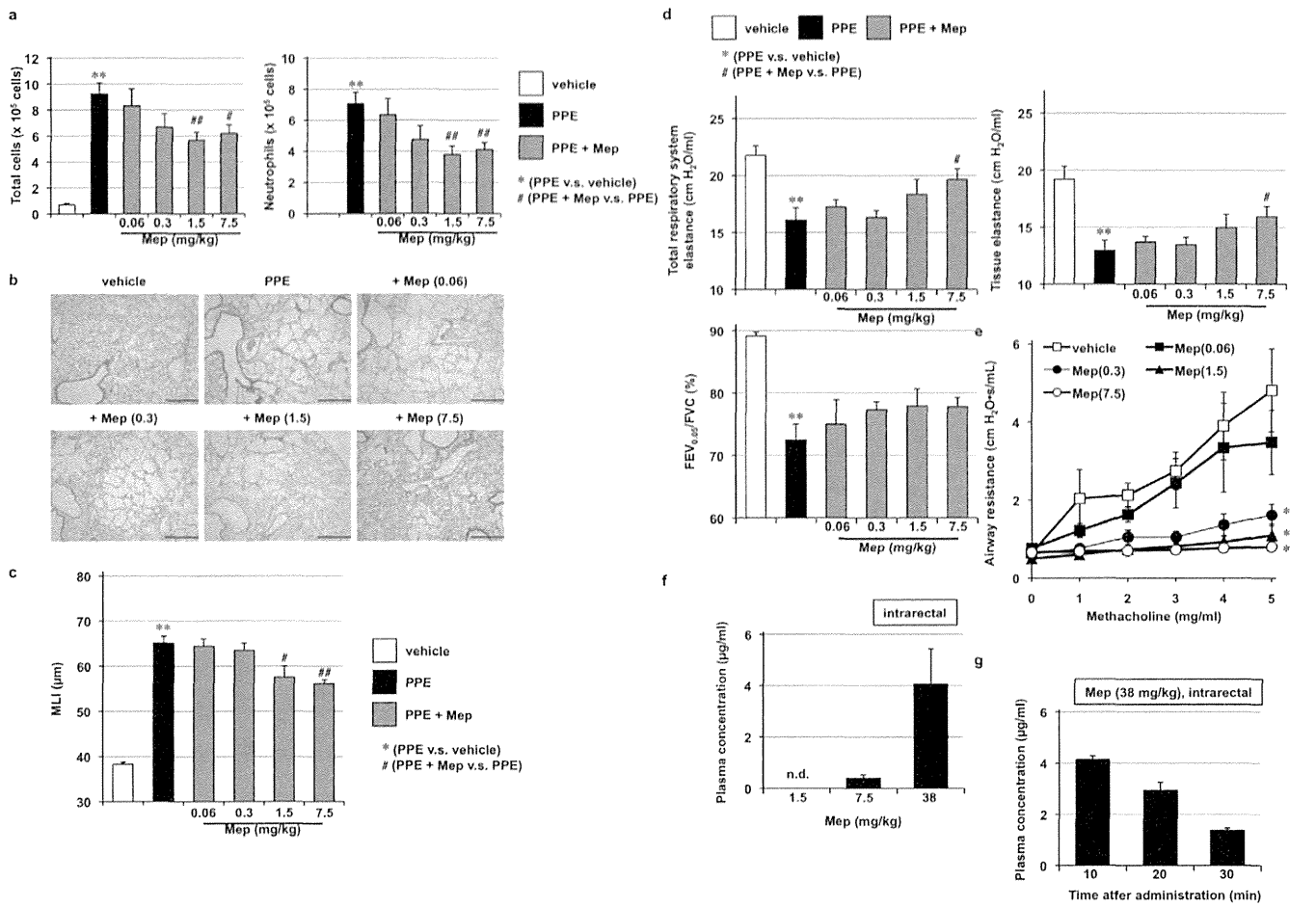

Figure 5 | Effect of intrarectal administration of mepenzolate on PPE-induced pulmonary damage and methacholine-induced airway constriction. Administration of PPE, mepenzolate and methacholine was done, as described in the legend of Fig. 1, except that mepenzolate was administered intrarectally (a–e). Analysis of inflammatory responses (a), histopathological examination (scale bar, 500 μm) (b), determination of the MLI (c), measurement of lung mechanics and respiratory function (d) and measurement of airway resistance (e) were carried out as described in the legend of Fig. 1. Mice were administered indicated doses of mepenzolate intrarectally. After 10 min (f) or indicated periods (g), blood samples were taken and the plasma level of mepenzolate was monitored as described in the legend of Fig. 4. Values represent mean ± S.E.M. ($n = 4$–12). * or $^{\#}$ $P < 0.05$; ** or $^{\#\#}$ $P < 0.01$; n.d., not detected.

the effective dose of mepenzolate was decreased. However, as for the oral and intravenous routes of administration, intrarectally administered mepenzolate exerted both beneficial and adverse side-effects at roughly similar doses.

To determine the appropriate administration route of candidate drugs in a clinical setting, the most important factor is the balance between efficacy and safety. To estimate this factor in animals, the ratio between doses showing adverse effects and efficacy is useful. We calculated this index (Table 1) and results show the superiority of the pulmonary administration route for mepenzolate compared to other routes. The quality of life (QOL) of patients is also an important factor, for which the intravenous route of administration has a disadvantage. As well as oral administration, pulmonary administration (such as inhalation) would not overly affect the QOL of COPD patients given that most of these patients would already be required to take bronchodilators and/or steroids on a daily basis at home through inhalation.

On the other hand, one of the main advantages of the oral route of mepenzolate administration is that it already has regulatory approval, and most pre-clinical tests (such as toxicity and pharmacokinetic tests) could be omitted if the dose for a new indication (COPD) is less than that for the approved indication (gastrointestinal disorders). However, we found that the dose of orally administered drug required to protect against PPE-induced pulmonary damage was much higher than that at which fecal pellet output is affected, suggesting that the clinical dose of mepenzolate for the treatment of COPD would be higher than the already approved dosage. On the other hand, if mepenzolate is developed as a drug to be administered via the pulmonary route, although some pre-clinical tests (such as toxicity and pharmacokinetic tests) are required, other tests (such as genotoxicity tests) could be omitted. Furthermore, because the dose required to protect against PPE-induced pulmonary damage via the intratracheal route was much lower than the orally administered dose that affects fecal pellet output, it could be postulated that the clinical dose of mepenzolate required for the treatment of COPD patients may be lower than the already approved dose if this drug is developed as a drug to be administered intrapulmonary. This could decrease the risk of adverse effects in a clinical setting. In conclusion, we propose that the pulmonary administration of mepenzolate may be superior to other administration routes for the treatment of COPD.

Methods

Chemicals and animals. Mepenzolate, PPE and HPLC-grade acetonitrile were obtained from Sigma-Aldrich (St. Louis, MO). Novo-Heparin for injection was from Mochida Pharmaceutical Co. (Tokyo, Japan). Chloral hydrate was from Nacalai Tesque (Kyoto, Japan). Diff-Quik was from the Sysmex Co (Kobe, Japan). Sodium 1-propanesulfonate was from Tokyo Kasei Chemical Co (Tokyo, Japan). The Amicon utra-0.5 centrifugal filter unit was purchased from Merck Millipore (Billerica, MA).

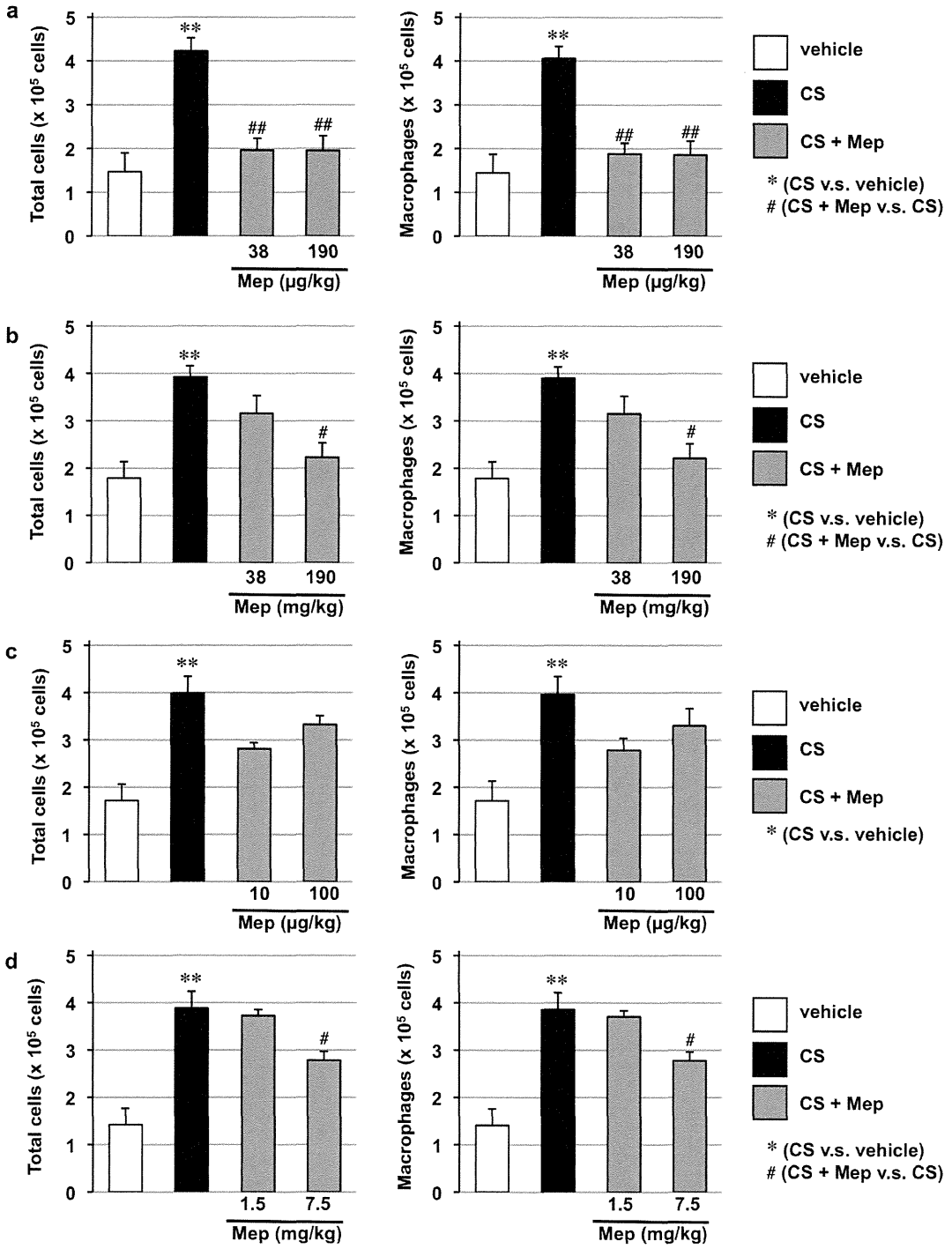

Figure 6 | Effect of mepenzolate on CS-induced pulmonary inflammatory responses. Mice were exposed to CS (3 times/day) and intratracheally (a), orally (b), intravenously (c) or intrarectally (d) administered indicated dose of mepenzolate (once daily) for 3 days as described in the Materials and Methods. Six hours after the last CS exposure, BALF was prepared and the total cell number and the number of macrophages were determined as described in the Materials and Methods. Values represent mean ± S.E.M. (n = 4–8). * or $^{\#}P < 0.05$; ** or $^{\#\#}P < 0.01$.

Formalin neutral buffer solution, potassium dihydrogen phosphate and methylcellulose were from WAKO Pure Chemicals (Tokyo, Japan). Mayer's hematoxylin, 1% eosin alcohol solution and malinol were from MUTO Pure Chemicals (Tokyo, Japan). ICR mice (4–6 weeks old, male) were purchased from Charles River (Yokohama, Japan). The experiments and procedures described here were carried out in accordance with the Guide for the Care and Use of Laboratory Animals as adopted and promulgated by the National Institutes of Health, and were approved by the Animal Care Committee of Keio University.

Treatment of mice with PPE, CS and drugs. Mice maintained under anesthesia with chloral hydrate (500 mg/kg) were given one intratracheal administration of PPE (15 U/kg) and mepenzolate (various doses) in PBS (1 ml/kg) via micropipette. For control mice, PBS alone was administered by the same procedure.

ICR mice were exposed to CS by placing 15–20 mice in a chamber (volume, 45 L) connected to a CS-producing apparatus. Commercial non-filtered cigarettes (Peace®; Japan Tobacco Inc., Tokyo, Japan) that yielded 28 mg tar and 2.3 mg nicotine on a standard smoking regimen were used. Mice were exposed to the smoke of 2 cigarettes for 20 min, 3 times/day for 3 days. The apparatus was configured such that each cigarette was puffed 15 times over a 5 min period.

For the oral or intrarectal mode of administration, mepenzolate (various doses) in 1% methylcellulose was administered by sonde. For control mice, 1% methylcellulose alone was administered by the same procedure.

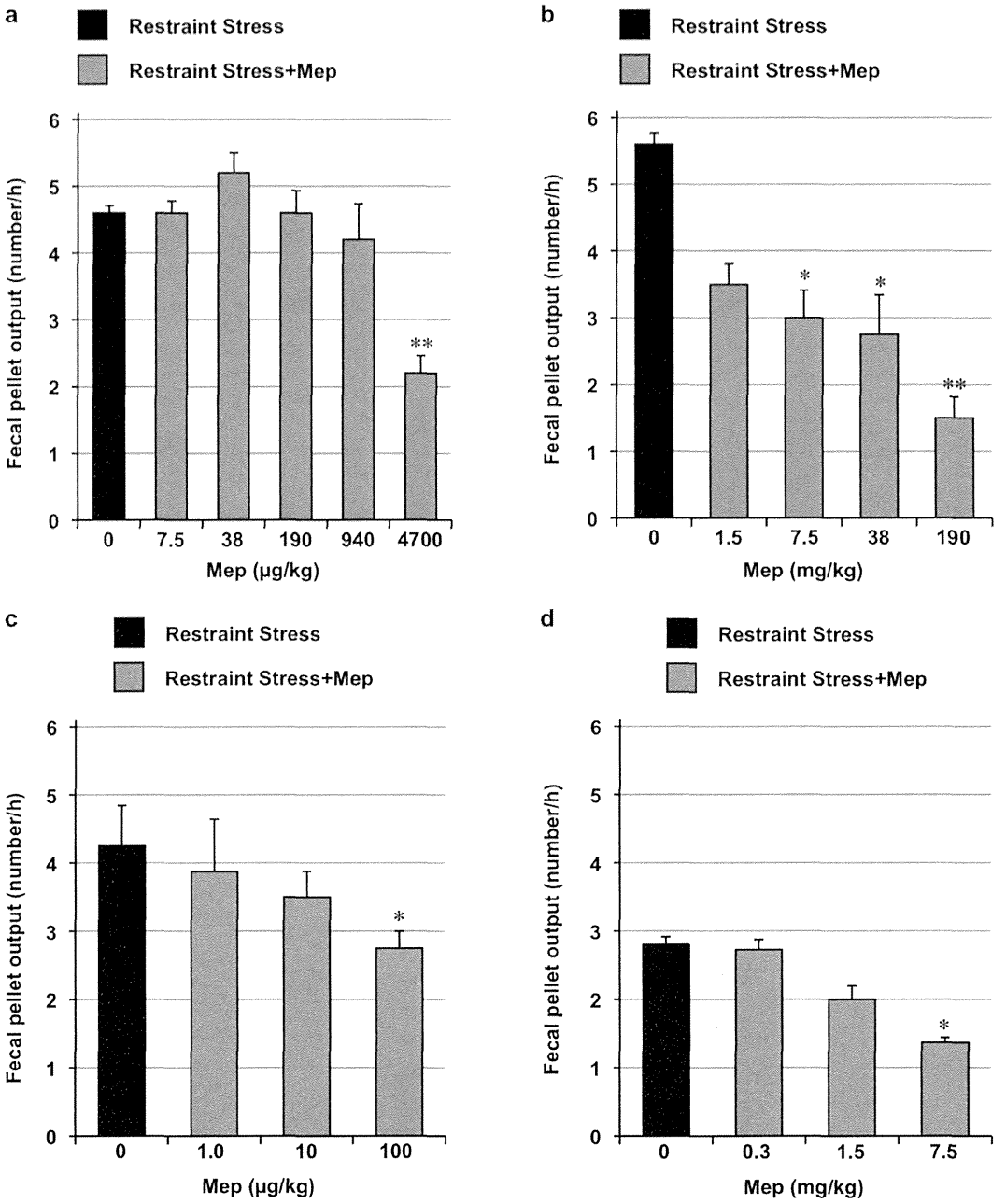

Figure 7 | Effect of mepenzolate on fecal pellet output. Mice were administered indicated doses of mepenzolate intratracheally (a), orally (b), intravenously (c) or intrarectally (d). One hour later, mice were exposed to restraint stress. The number of fecal pellets excreted during the restraint stress period (1 h) was determined. Values represent mean ± S.E.M. (n = 4–15). * $P < 0.05$; ** $P < 0.01$.

For the intravenous administration of mepenzolate, mice were maintained under anesthesia with chloral hydrate (500 mg/kg) and mepenzolate (various doses) in PBS was administered by syringe via a 26 G needle (TERUMO, Tokyo, Japan). For control mice, PBS alone was administered by the same procedure.

At day 0, the administration of mepenzolate was performed 1 h (intratracheal administration) or 0.5 h (other routes of administration) prior to the PPE administration or the CS exposure.

Preparation of BALF and cell count method. BALF was collected by cannulating the trachea and lavaging the lung with 1 ml of sterile PBS containing 50 U/ml heparin (2 times). About 1.8 ml of BALF was routinely recovered from each animal. The total cell number was counted using a hemocytometer. Cells were stained with Diff-Quik reagents after centrifugation with Cytospin® 4 (Thermo Electron Corporation, Waltham, MA), and the ratio of number of neutrophils to total cell number was examined to determine the number of neutrophils.

Histopathological analysis. Lung tissue samples were fixed in 10% formalin neutral buffer solution for 24 h at a pressure of 25 cmH_2O, and then embedded in paraffin before being cut into 4 μm-thick sections. Sections were stained first with Mayer's hematoxylin and then with 1% eosin alcohol solution (H & E staining). Samples were mounted with malinol and inspected with the aid of an Olympus BX51 microscope (Tokyo, Japan).

To determine the MLI (an indicator of airspace enlargement), 20 lines (500 μm) were drawn randomly on the image of a section and intersection points with alveolar walls were counted to determine the MLI. This morphometric analysis was conducted by an investigator blinded to the study protocol.

Measurement of lung mechanics, airway resistance and $FEV_{0.05}$/FVC. Lung mechanics and airway resistance were monitored with a computer-controlled small-animal ventilator (FlexiVent, SCIREQ, Montreal, Canada), as described previously[18,19]. Mice were anesthetized with chloral hydrate (500 mg/kg), a tracheotomy was performed, and an 8 mm section of metallic tube was inserted into the trachea. Mice were mechanically ventilated at a rate of 150 breaths/min, using a tidal volume of 8.7 ml/kg and a positive end-expiratory pressure of 2–3 cmH_2O.

Total respiratory system elastance and tissue elastance were measured by the snapshot and forced oscillation techniques, respectively. All data were analysed using FlexiVent software (version 5.3; SCIREQ, Montreal, Canada).

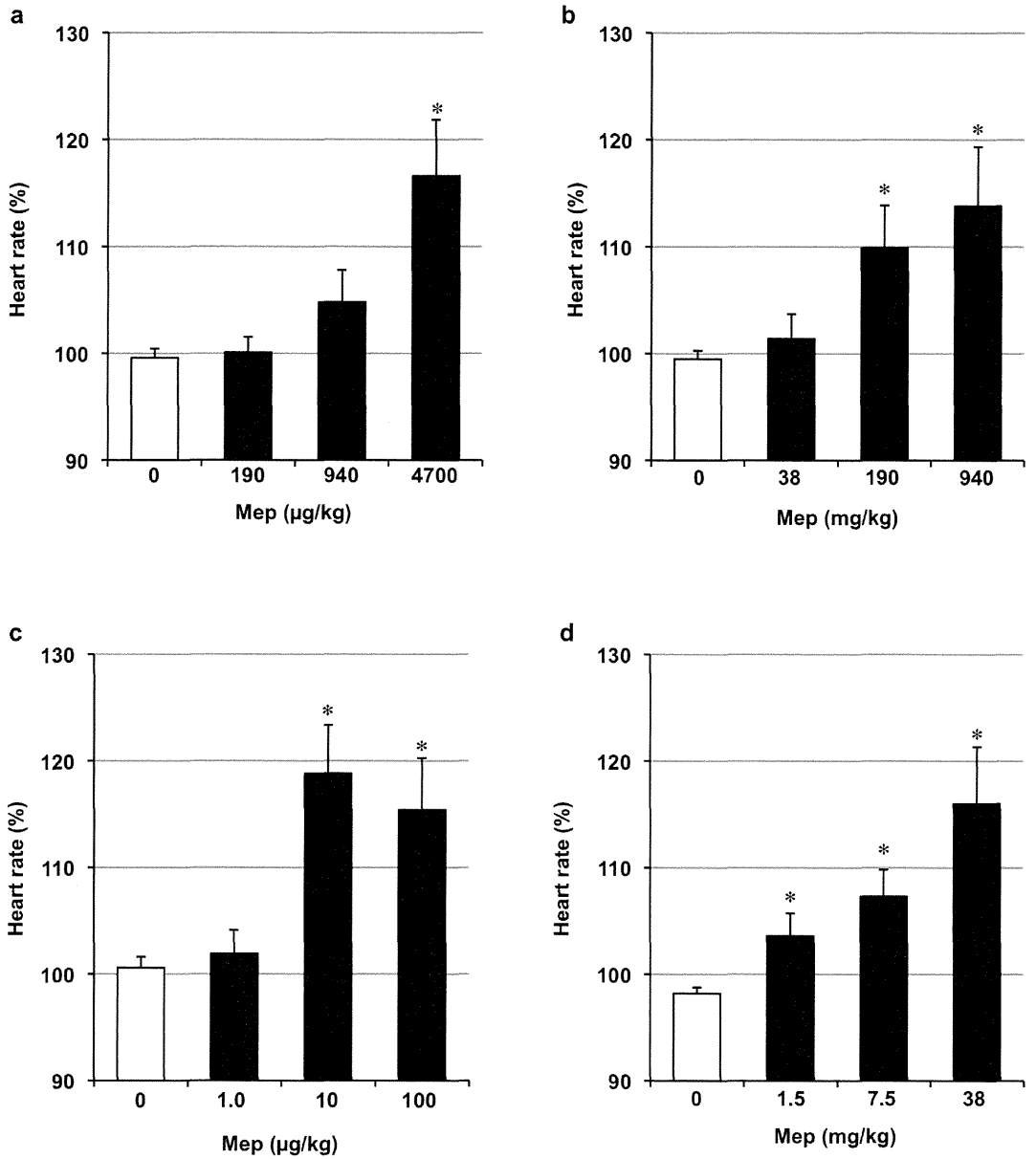

Figure 8 | Effect of mepenzolate on heart rate. Mice were administered indicated doses of mepenzolate intratracheally (a), orally (b), intravenously (c) or intrarectally (d). The alteration of heart rate (beats per minute) by the mepenzolate administration was monitored as described in the Materials and Methods. Mepenzolate-dependent alteration of heart rate from the baseline to the peak is shown. Values represent mean ± S.E.M. ($n = 3$–7). * $P < 0.05$; ** $P < 0.01$.

For measurement of methacholine-induced increases in airway resistance, mice were exposed to nebulized methacholine (1 mg/ml) five times for 20 sec with a 40 sec interval, and airway resistance was measured after each methacholine challenge by the snapshot technique. All data were analysed using the FlexiVent software.

Determination of the FEV0.05/FVC (forced expiratory volume in the first 0.05 seconds to forced vital capacity) ratio was performed with the same computer-controlled small-animal ventilator connected to a negative pressure reservoir (SCIREQ, Montreal, Canada), as described previously[18,19]. Mice were tracheotomised and ventilated as described above. The lung was inflated to 30 cmH_2O over one second and held at this pressure. After 0.2 sec, the pinch valve (connected to ventilator) was closed and after 0.3 sec, the shutter valve (connected to negative pressure reservoir) was opened for exposure of the lung to the negative pressure. The negative pressure was held for 1.5 sec to ensure complete expiration. FEV0.05/FVC was determined using the FlexiVent software.

Table 1 | Efficacy versus toxicity ratio for different routes of mepenzolate administration

Administration route	Intratracheal	Oral	Intravenous	Intrarectal
Efficacy	38 μg/kg	190 mg/kg	10 μg/kg	1.5 mg/kg
Toxicity	4700 μg/kg	7.5 mg/kg	10 μg/kg	1.5 mg/kg
Toxicity/Efficacy	120	0.04	1	1

The effective dose (efficacy) was determined as the minimum dose required to significantly suppress the PPE-induced increase in MLI (Figs. 1c, 2c, 3c and 5c). The toxic dose (toxicity) was determined as the minimum dose required to significantly affect either fecal pellet output or heart rate (Figs. 7 and 8). The ratio of the toxic dose versus the effective dose for each route of administration is shown.

Analysis of fecal pellet output. Mice were subjected to restraint stress by being placed individually into a 50 ml tube (Becton Dickinson, Franklin Lakes, NJ) for 1 h, as described previously[28]. These tubes are small enough to restrain a mouse so that it is able to breathe but unable to move freely. The number of fecal pellets excreted during the restraint stress period (1 h) was measured.

Measurement of heart rate. Heart rate was measured with a MouseOx system (STARR Life Sciences Corp., Allison Park, PA), as described previously[29]. Mice were anesthetized with chloral hydrate (500 mg/kg) and the sensor was attached to the thigh. Heart rate was determined using MouseOx software (STARR Life Sciences Corp., Allison Park, PA).

Determination of the level of mepenzolate in vivo. After administration of mepenzolate, blood samples (800 μl) were taken periodically into centrifuge tubes containing heparin (50 μl) and centrifuged immediately (1000 × g, 10 min) to obtain the sample. Whole lungs were taken from mepenzolate-treated mice, homogenised in sterile PBS containing 50 U/ml heparin, and centrifuged (14, 000 × g, 1 min) to obtain the sample. An aliquot (300 μl) of each sample was ultrafiltered with an Amicon utra-0.5 centrifugal filter to extract the mepenzolate. The filtrate was analysed by analytical HPLC with a reverse-phase column (TSKgel Super-ODS, 150 × 4.6 mm, 2 μm, Tosoh Co., Tokyo, Japan), Waters 2695 Alliance separation module, and a Waters 2996 photodiode array detector (Waters, Milford, MA). Solution containing 30% (v/v) acetonitrile and 14 mM potassium dihydrogen phosphate/sodium 1-propanesulfonate buffer was used at a flow rate of 0.3 ml/min. Detection was performed at an optical density of 220 nm.

Statistical analysis. All values are expressed as the mean ± S.E.M. Two-way ANOVA followed by the Tukey test or the Student's *t*-test for unpaired results was used to evaluate differences between three or more groups or between two groups, respectively. Differences were considered to be significant for values of $P < 0.05$.

1. Rabe, K. F. *et al.* Global strategy for the diagnosis, management, and prevention of chronic obstructive pulmonary disease: GOLD executive summary. *Am J Respir Crit Care Med* **176**, 532–555 (2007).
2. Barnes, P. J. & Stockley, R. A. COPD: current therapeutic interventions and future approaches. *Eur Respir J* **25**, 1084–1106 (2005).
3. Owen, C. A. Proteinases and oxidants as targets in the treatment of chronic obstructive pulmonary disease. *Proc Am Thorac Soc* **2**, 373–385; discussion 394–375 (2005).
4. Tashkin, D. P. *et al.* A 4-year trial of tiotropium in chronic obstructive pulmonary disease. *N Engl J Med* **359**, 1543–1554 (2008).
5. Calverley, P. M. *et al.* Salmeterol and fluticasone propionate and survival in chronic obstructive pulmonary disease. *N Engl J Med* **356**, 775–789 (2007).
6. Alsaeedi, A., Sin, D. D. & McAlister, F. A. The effects of inhaled corticosteroids in chronic obstructive pulmonary disease: a systematic review of randomized placebo-controlled trials. *Am J Med* **113**, 59–65 (2002).
7. Barnes, P. J., Ito, K. & Adcock, I. M. Corticosteroid resistance in chronic obstructive pulmonary disease: inactivation of histone deacetylase. *Lancet* **363**, 731–733 (2004).
8. Mizushima, T. Drug discovery and development focusing on existing medicines: drug re-profiling strategy. *J Biochem* **149**, 499–505 (2011).
9. Tanaka, K. *et al.* Mepenzolate bromide displays beneficial effects in a mouse model of chronic obstructive pulmonary disease. *Nat Commun* **4**, (2013).
10. Chen, J. Y. Antispasmodic activity of JB-340 (N-methyl-3-piperidyl-diphenylglycolate methobromide) with special reference to its relative selective action on the sphincter of Oddi, colon and urinary bladder of the dog. *Arch Int Pharmacodyn Ther* **121**, 78–84 (1959).
11. Buckley, J. P., De, F. J. & Reif, E. C. The comparative antispasmodic activity of N-methyl-3-piperidyl diphenylglycolate methobromide (JB-340) and atropine sulfate. *J Am Pharm Assoc Am Pharm Assoc (Baltim)* **46**, 592–594 (1957).
12. Long, J. P. & Keasling, H. H. The comparative anticholinergic activity of a series of derivatives of 3-hydroxy piperidine. *J Am Pharm Assoc Am Pharm Assoc (Baltim)* **43**, 616–619 (1954).
13. Drummond, G. R., Selemidis, S., Griendling, K. K. & Sobey, C. G. Combating oxidative stress in vascular disease: NADPH oxidases as therapeutic targets. *Nat Rev Drug Discov* **10**, 453–471 (2011).
14. Gosker, H. R. *et al.* Altered antioxidant status in peripheral skeletal muscle of patients with COPD. *Respir Med* **99**, 118–125 (2005).
15. Rahman, I. & MacNee, W. Antioxidant pharmacological therapies for COPD. *Curr Opin Pharmacol* **12**, 256–265 (2012).
16. Prat, M., Gavalda, A., Fonquerna, S. & Miralpeix, M. Inhaled muscarinic antagonists for respiratory diseases: a review of patents and current developments (2006–2010). *Expert Opin Ther Pat* **21**, 1543–1573 (2011).
17. Kuraki, T., Ishibashi, M., Takayama, M., Shiraishi, M. & Yoshida, M. A novel oral neutrophil elastase inhibitor (ONO-6818) inhibits human neutrophil elastase-induced emphysema in rats. *Am J Respir Crit Care Med* **166**, 496–500 (2002).
18. Tanaka, K. *et al.* Therapeutic effect of lecithinized superoxide dismutase on pulmonary emphysema. *J Pharmacol Exp Ther* **338**, 810–818 (2011).
19. Tanaka, K., Sato, K., Aoshiba, K., Azuma, A. & Mizushima, T. Superiority of PC-SOD to other anti-COPD drugs for elastase-induced emphysema and alteration in lung mechanics and respiratory function in mice. *Am J Physiol Lung Cell Mol Physiol* **302**, L1250–1261 (2012).
20. Bergogne-Berezin, E. & Bryskier, A. The suppository form of antibiotic administration: pharmacokinetics and clinical application. *J Antimicrob Chemother* **43**, 177–185 (1999).
21. Sasaki, K., Yonebayashi, S., Yoshida, M., Shimizu, K., Aotsuka, T. & Takayama, K. Improvement in the bioavailability of poorly absorbed glycyrrhizin via various non-vascular administration routes in rats. *Int J Pharm* **265**, 95–102 (2003).
22. Agarwal, R. & Jindal, S. K. Acute exacerbation of idiopathic pulmonary fibrosis: a systematic review. *Eur J Intern Med* **19**, 227–235 (2008).
23. Verhamme, K. M. *et al.* Tiotropium Handihaler and the risk of cardio- or cerebrovascular events and mortality in patients with COPD. *Pulm Pharmacol Ther* **25**, 19–26 (2012).
24. Gross, N. J., Giembycz, M. A. & Rennard, S. I. Treatment of chronic obstructive pulmonary disease with roflumilast, a new phosphodiesterase 4 inhibitor. *COPD* **7**, 141–153 (2010).
25. Miravitlles, M. & Anzueto, A. Insights into interventions in managing COPD patients: lessons from the TORCH and UPLIFT studies. *Int J Chron Obstruct Pulmon Dis* **4**, 185–201 (2009).
26. Rajendrasozhan, S., Yang, S. R., Edirisinghe, I., Yao, H., Adenuga, D. & Rahman, I. Deacetylases and NF-kappaB in redox regulation of cigarette smoke-induced lung inflammation: epigenetics in pathogenesis of COPD. *Antioxid Redox Signal* **10**, 799–811 (2008).
27. Ito, K. *et al.* Histone deacetylase 2-mediated deacetylation of the glucocorticoid receptor enables NF-kappaB suppression. *J Exp Med* **203**, 7–13 (2006).
28. Asano, T. *et al.* Effects of beta-(1,3-1,6)-D-glucan on irritable bowel syndrome-related colonic hypersensitivity. *Biochem Biophys Res Commun* **420**, 444–449 (2012).
29. McLaughlin, B., Buendia, M. A., Saborido, T. P., Palubinsky, A. M., Stankowski, J. N. & Stanwood, G. D. Haploinsufficiency of the E3 ubiquitin ligase C-terminus of heat shock cognate 70 interacting protein (CHIP) produces specific behavioral impairments. *PLoS One* **7**, e36340 (2012).

Acknowledgments

We thank Dr. Tomoko Betsuyaku (Keio University) for helpful discussion and Mrs. Kumi Matsuura (Kumamoto University) for technical assistance. This work was supported by Grants-in-Aid for Scientific Research from the Ministry of Health, Labour, and Welfare of Japan, as well as the Japan Science and Technology Agency and Grants-in-Aid for Scientific Research from the Ministry of Education, Culture, Sports, Science and Technology, Japan.

Author contributions

Conception and design: K.T. and T.M.; Analysis and interpretation: K.T., T.A., N.Y., D.K., Y.Y., H.Y., S.K. and T.I.; Drafting the manuscript for important intellectual content: K.T., T.A., N.Y., H.W., T.M., H.S. and T.M.

Additional information

Competing financial interests: The authors declare no competing financial interests.

How to cite this article: Tanaka, K.-I. *et al.* Superiority of pulmonary administration of mepenzolate bromide over other routes as treatment for chronic obstructive pulmonary disease. *Sci. Rep.* **4**, 4510; DOI:10.1038/srep04510 (2014).

RHEUMATOLOGY

Rheumatology 2015;54:349–358
doi:10.1093/rheumatology/keu325
Advance Access publication 28 August 2014

Original article

Proteomic identification of heterogeneous nuclear ribonucleoprotein K as a novel cold-associated autoantigen in patients with secondary Raynaud's phenomenon

Lingli Yang[1,2], Minoru Fujimoto[2], Hiroyuki Murota[1], Satoshi Serada[2], Manabu Fujimoto[3], Hiromi Honda[2], Kohji Yamada[2,4], Katsuya Suzuki[5], Ayumi Nishikawa[5], Yuji Hosono[6], Yoshihiro Yoneda[7], Kazuhiko Takehara[3], Yoshitaka Imura[6], Tsuneyo Mimori[6], Tsutomu Takeuchi[5], Ichiro Katayama[1] and Tetsuji Naka[2]

Abstract

Objective. The aim of this study was to identify cold-associated autoantibodies in patients with RP secondary to CTDs.

Methods. Indirect immunofluorescence staining was performed on non-permeabilized cold-stimulated normal human dermal microvascular endothelial cells (dHMVECs), using patients' sera. Cold-induced alterations in cell surface proteomes were analysed by isobaric tag for relative and absolute quantitation (iTRAQ) analysis. Serological proteome analysis (SERPA) was applied to screen cold-associated autoantigens. The prevalence of the candidate autoantibody was determined by ELISA in 290 patients with RP secondary to CTDs (SSc, SLE or MCTD), 10 patients with primary RP and 27 healthy controls.

Results. Enhanced cell surface immunoreactivity was detected in cold-stimulated dHMVECs when incubated with sera from patients with secondary RP. By iTRAQ analysis, many proteins, including heterogeneous nuclear ribonucleoprotein K (hnRNP-K), were found to be increased on the cell surface of dHMVECs after cold stimulation. By the SERPA approach, hnRNP-K was identified as a candidate autoantigen in patients with secondary RP. Cold-induced translocation of hnRNP-K to the cell surface was confirmed by immunoblotting and flow cytometry. By ELISA analysis, patients with secondary RP show a significantly higher prevalence of anti-hnRNP-K autoantibody (30.0%, 61/203) than patients without RP (9.2%, 8/87, $P=0.0001$), patients with primary RP (0%, 0/10, $P=0.0314$) or healthy controls (0%, 0/27, $P=0.0001$).

Conclusion. By comprehensive proteomics, we identified hnRNP-K as a novel cold-associated autoantigen in patients with secondary RP. Anti-hnRNP-K autoantibody may potentially serve as a biomarker for RP secondary to various CTDs.

Key words: proteomics, Raynaud's phenomenon, autoantibody, heterogeneous nuclear RNP-K.

[1]Department of Dermatology, Osaka University Graduate School of Medicine, [2]Laboratory of Immune Signal, National Institute of Biomedical Innovation, [3]Department of Dermatology, Kanazawa University, Kanazawa, [4]Biomolecular Dynamics Group, Graduate School of Frontier Biosciences, Osaka University, Osaka, [5]Division of Rheumatology, Department of Internal Medicine, Keio University School of Medicine, Tokyo, [6]Department of Rheumatology and Clinical Immunology, Graduate School of Medicine, Kyoto University, Kyoto and [7]National Institute of Biomedical Innovation, Osaka, Japan.

Submitted 4 November 2013; revised version accepted 23 June 2014.

Correspondence to: Tetsuji Naka, Laboratory of Immune Signal, National Institute of Biomedical Innovation, 7-6-8, Saito-asagi, Ibaraki, Osaka 567-0085, Japan. E-mail: tnaka@nibio.go.jp

Lingli Yang, Minoru Fujimoto, Hiroyuki Murota and Satoshi Serada contributed equally to this study.

Introduction

Advances in proteomics technologies have enabled us to identify proteins extracted from various clinical samples. Recently an innovative multiplexed quantitative proteomic technology called isobaric tag for relative and absolute quantification (iTRAQ) has been successfully used to detect disease-related proteins from cultured cells and clinical samples [1]. This novel technology can not only identify proteins in samples, but also compare relative expression levels of detected proteins from between four to eight different samples [2]. In addition, when samples enriched with cell surface proteins are analysed, iTRAQ technology can characterize differences in cell surface proteomes between samples [3].

RP is an exaggerated vasoconstrictive response of the fingers and toes to external stress such as cold temperatures [4]. RP is characterized classically as the episodic colour change of blanching, cyanosis and rubor in response to external stress [5]. In most patients, this colour change is a benign, reversible condition and no underlying disease is detectable (i.e. primary RP) [4]. However, in some patients RP is the early manifestation of underlying disease (i.e. secondary RP), most frequently of CTDs, including SSc [4], SLE [6] and MCTD [7]. RP in CTD patients is more severe than primary RP and causes tissue damage, including digital ulcers and gangrene, presumably due to endothelial abnormalities [8]. Moreover, given the substantial morbidity in patients with CTDs, RP patients developing CTDs should be promptly identified and managed. Thus it is important to distinguish between primary and secondary RP, but the diagnostic methods have not been established.

Because autoantibody production is a common hallmark of CTDs, RP secondary to CTDs might have a similar autoimmune pathogenesis. We therefore hypothesized that cold stimulation, as an environmental cue, may contribute to the triggering of local autoimmune reactions in patients with CTD-related secondary RP. In this study, taking advantage of iTRAQ technology, we detected cold-induced alteration in cell surface proteomes of endothelial cells. We then obtained candidate autoantigens in RP by serological proteome analysis (SERPA) [9–11] combining two-dimensional electrophoresis and western blotting using patients' sera. Our analyses collectively suggest that in patients with secondary RP, heterogeneous nuclear ribonucleoprotein K (hnRNP-K) is a cold-associated autoantigen that translocates onto the cell surface by cold stimulation.

Materials and methods

Human serum samples

Between March 2003 and January 2012, Japanese patients referred to hospitals of Osaka University (Osaka, Japan), Kyoto University (Kyoto, Japan), Kanazawa University (Kanazawa, Japan) and Keio University (Tokyo, Japan) were newly evaluated for RP as well as for SSc according to ACR criteria [12], SLE according to ACR criteria [13, 14] or MCTD according to the criteria proposed by the Ministry of Health and Welfare in Japan [15]. RP was defined by repeated episodes of biphasic or triphasic colour change on cold exposure and non-RP was defined by no colour changes on cold exposure, as described previously [16]. The possible RP of unilateral or uniphasic colour change was not included in this study. After these exclusions, randomly selected patients, including 155 well-defined SSc with RP [SSc-RP(+)] patients, 54 SLE without RP [SLE-RP(−)] patients, 1 MCTD without RP [MCTD-RP(−)] patient and 10 MCTD with RP [MCTD-RP(+)] patients, were included in this study. SSc without RP [SSc-RP(−)] patients ($n = 32$) and SLE with well-defined RP [SLE-RP(+)] ($n = 38$) patients, the frequencies of which are substantially low, were intentionally recruited and included in the study. Sera and characteristics (demographic characteristics, autoantibody profile) of CTD patients were collected at the time of diagnosis. Ten patients with primary RP who had well-defined RP for >2 years and had normal findings on laboratory tests, negative findings on autoantibody assays and no objective clinical signs of CTD or other diseases were also included. These patient characteristics are summarized in Table 1. As controls, healthy individuals with no evidence of any physical disorder were included [$n = 27$; male:female ratio 3:24, average age 51.0 years (S.D. 13.2)]. All patients gave written informed consent prior to inclusion and this study was approved by the Medical Ethics Committees of the National Institute of Biomedical Innovation (Osaka, Japan), Osaka University Hospital, Kyoto University Hospital, Kanazawa University Hospital and Keio University Hospital.

Cell culture and cold stimulation

Normal human dermal microvascular (MV) endothelial cells (dHMVECs, passages 4–6) were purchased from Takara Bio (Otsu, Japan). dHMVECs were cultured on type 1 collagen-coated plates (Iwaki Glass, Tokyo, Japan) in endothelial basal medium 2 supplemented with endothelial cell growth medium 2 MV SingleQuots (Clonetics, San Diego, CA, USA). Confluent dHMVECs cells were incubated in serum-containing medium at 10°C (cold stress) or 37°C (control) in a 5% CO_2 humidified incubator for the periods indicated. Cells were maintained at 10°C or 37°C during the washing/detachment procedure. Suspended cells were then harvested by centrifugation at room temperature. Before and after cold stimulation, cell viability was verified by trypan blue exclusion assay. In some experiments, cells were further fixed with 4% paraformaldehyde at room temperature.

Indirect immunofluorescence staining

dHMVECs were seeded on six-well plates precoated with type 1 collagen (5×10^4 cells/well) and grown to confluence. Cells were fixed with 4% paraformaldehyde. Non-permeabilized cells were then incubated with sera from patients and healthy controls (HCs; 1:500 dilution) for 1 h at room temperature, followed by incubation with FITC-conjugated rabbit anti-human IgG (1:1000 dilution;

TABLE 1 Patient characteristics ($n = 300$ with CTDs or primary RP)

Variable	SSc ($n = 187$)	SLE ($n = 92$)	MCTD ($n = 11$)	Primary RP ($n = 10$)
Age, mean (S.D.), years	55.3 (13.8)	40.3 (14.9)	59.5 (16.3)	25.4 (3.1)
Gender (F:M), *n:n*	156:31	86:6	11:0	9:1
Smoking, % (*n/N*)	44.2 (50/163)	25.8 (16/46)	0 (0/11)	0 (0/10)
ANA positivity, % (n/N)	91.4 (167/183)	96.7 (89/92)	100 (10/10)	0 (0)
Anti-Scl-70, % (*n/N*)	31.0 (58/187)	NA	NA	0 (0/10)
Anti-centromere, % (*n/N*)	33.7 (63/187)	NA	9.1 (1/11)	0 (0/10)
Anti-Sm, % (*n/N*)	NA	34.5 (30/87)	9.1 (1/11)	NA
Anti-dsDNA, % (*n/N*)	NA	65.1 (54/83)	0 (0/3)	NA
Anti-U1-RNP, % (*n/N*)	7.5 (14/187)	50.0 (43/86)	100.0 (11/11)	0 (0/10)
Anti-SSA/Ro, % (*n/N*)	7.5 (14/187)	57.8 (52/87)	45.5 (5/11)	NA

Scl-70: topoisomerase I; Sm: Smith; U1-RNP: U1 ribonucleoprotein; *N*: the number of available patients (varies according to the number of available observations); NA: not available.

Dako Immunoglobulins, Copenhagen, Denmark). Cells counterstained with Hoechst 33342 (Invitrogen, Carlsbad, CA, USA) were visualized using a Biozero microscope (Keyence, Itasca, IL, USA).

Capture of cell surface proteins

After cold stimulation (10°C) for the indicated periods (0 min, 30 min, 1 h, 3 h), dHMVECs were washed with pre-warmed (37°C) or precooled (10°C) PBS three times and cell surface proteins were then labelled by biotinylation and pulled down by avidin–agarose resin as described previously [3]. The isolated cell surface proteins were kept at −20°C until use.

iTRAQ analysis

Cell surface proteins described above were digested by trypsin and separately labelled with the iTRAQ reagent (Applied Biosystems, Foster City, CA, USA) as described previously [3]. Briefly, iTRAQ reagents 114–117 were used to label cells without cold stimulation (baseline), cells with cold stimulation at 10°C for 30 min, cells with cold stimulation at 10°C for 1 h and cells with cold stimulation at 10°C for 3 h, respectively. Samples were then pooled and fractionated by strong cation exchange chromatography [3]. Nano liquid chromatography–tandem mass spectrometry (LC-MS/MS) analyses were performed on an LTQ-Orbitrap XL (Thermo Fisher Scientific, Waltham, MA, USA) as described previously [3]. Protein identification and quantification for iTRAQ analysis were carried out using Proteome Discoverer software (version 1.1; Thermo Fisher Scientific) against the Swiss Prot protein database [SwissProt 2010_10 (521 016 sequences)] as described previously [3] with modifications as follows: carbamidomethylation and iTRAQ4plex (Lys, N-terminal) were specified as static modifications, whereas CAMthiopropanoyl (Lys, N-terminal), iTRAQ4plex (Tyr) and oxidation (Met) were specified as variable modifications in the database search. The mass spectrometry raw data and the data of peptide identifications were uploaded to PeptideAtlas (http://www.peptideatlas.org/PASS/PASS00387). Information about the subcellular localization of detected proteins was obtained by using UniprotKB (http://www.uniprot.org/).

Serological proteome analysis

Proteins were extracted from cultured dHMVECs using the Complete Mammalian Proteome Extraction Kit (Calbiochem, La Jolla, CA, USA) and stored at −80°C until use. Two-dimensional electrophoresis and immune blotting analysis using patient or HC sera were performed as previously described [10, 11]. Protein spots in a silver-stained gel, corresponding to positive spots on western blot membranes, were excised from the gel and digested in gel as described previously [17].

Preparation of recombinant human hnRNP-K

Full-length hnRNP-K cDNA was amplified from total cDNA of dHMVEC using KOD-plus (Toyobo, Osaka, Japan) with the following primers: 5′-TGGAAACTGAACAGCCAGAAG AA-3′ (forward) and 5′-GCATTAGAATCCTTCAACATCTG C-3′ (reverse). Full-length hnRNP-K cDNA was subcloned into a pET28 vector (Novagen, Madison, WI, USA), resulting in expression of hnRNP-K with a 6 × His tag. The DNA sequence was confirmed using the ABI Prism 3130XL Genetic Analyzer (Applied Biosystems). Recombinant protein was produced in *Escherichia coli* as described previously [10, 11].

ELISA

The ELISA assay was performed using MaxiSorp plates (Nunc A/S, Roskilde, Denmark) coated with 1 μg/well of recombinant human full-length hnRNP-K protein. After dilution (1:500) with *E. coli* cell lysates to block the non-specific reactivity of sera with bacterial proteins, sera were incubated with plate-bound hnRNP-K for 1 h, followed by detection of antigen–antibody complexes by horseradish peroxidase (HRP)-conjugated rabbit anti-human IgG (Dako, Carpinteria, CA, USA) as described previously [10, 11]. Optical density (OD) was read at 450 nm on a Model 680 Microplate Reader (Bio-Rad Laboratories, Hercules, CA, USA). The antibody titre was expressed using arbitrary binding units calculated

according to the following formula: binding units of sample = [OD_{sample}/(mean $OD_{HC\ sera}$ + 3 S.D.$_{HC\ sera}$)] × 100. Based on this formula, 100 binding units was used as the cut-off point.

Western blot analysis

Extracted proteins were subjected to western blot analysis as previously described [18] with the following antibodies: serum at 1:200 dilution; anti-hnRNP-K (1:500 dilution; Cell Signaling Technology, Danvers, MA, USA); anti-VE-cadherin (1:500 dilution; BD Transduction Laboratories, San Jose, CA, USA); anti-glyceraldehyde-3-phosphate dehydrogenase (GAPDH; 1:1000 dilution; Santa Cruz Biotechnology, Dallas, TX, USA), followed by rabbit anti-human IgG, donkey anti-rabbit or sheep anti-mouse HRP-conjugated secondary antibodies (1:5000 dilution; GE Healthcare, Piscataway, NJ, USA) and visualized with Western Lightning Plus ECL reagent (Perkin-Elmer, Boston, MA, USA).

Fluorescence-activated cell sorting

After stimulation, cells fixed with 4% paraformaldehyde were incubated with rabbit anti-human hnRNP-K antibody at 1:100 dilution and labelled with FITC-conjugated goat anti-rabbit immunoglobulin (BD Biosciences, San Jose, CA, USA). Normal rabbit IgG was used as a control. Stained cells were analysed using a FACS Canto II cytometer (Becton-Dickinson, Mountain View, CA, USA) and the results were analysed using FlowJo software (TreeStar, Ashland, OR, USA).

Statistical analysis

Continuous variables are expressed as mean (S.D.) and proportions were used for categorical variables. Means were compared with Student's *t*-test, highly skewed distributions were compared using the Mann–Whitney *U* test and proportions were compared using Fisher's exact test. Differences between groups were compared using the Kruskall–Wallis test followed by Steel's test. The data were entered and analysed using Excel statistical software (Microsoft, Redmond, WA, USA). Significance was defined as $P < 0.05$.

Results

Cold-induced autoimmune reactions on the cell surface

To determine whether cold can affect autoimmune reactions on the surface of vascular endothelial cells, non-permeabilized dHMVECs pretreated with or without cold stimulation were incubated with sera from patients with RP secondary to SSc or HCs. By indirect immunofluorescence staining using sera from patients, cell surface immunoreactivity was strongly induced in cold-stimulated dHMVECs (eight of nine patients with SSC-related RP; Fig. 1), but not in unstimulated cells. In contrast, no distinct immunostaining was observed in cold-stimulated or unstimulated cells when incubated with sera from HCs ($n = 3$; Fig. 1). These results indicate that pretreatment of dHMVECs with cold is critical in inducing the interaction between cell surface autoantigens and sera from patients.

FIG. 1 Indirect immunofluorescence staining

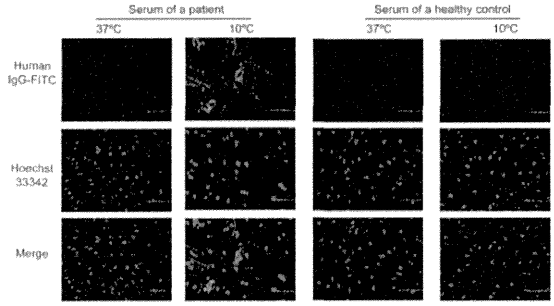

Non-permeabilized cultured dHMVECs with or without cold stimulation were incubated with sera (1:500 dilution) from patients with SSc-related secondary RP ($n = 9$) or healthy controls ($n = 3$) (×100 magnification). Representative images are shown here. FITC-conjugated rabbit anti-human IgG (green); Hoechst 33342 (blue); bar: 100 μm. dHMVECs: dermal human microvascular endothelial cells.

Identification of cold-induced surface proteome alterations in dHMVECs by iTRAQ analysis

The results above suggest that proteins including autoantigens in dHMVECs might be exposed to the cell surface in response to cold stimulation. Therefore we next investigated cold-induced cell surface proteome alterations in dHMVECs. Cells were stimulated with cold (10°C for 0 min, 30 min, 1 h and 3 h) and cell surface proteins enriched by a biotinylation-based approach were quantitatively analysed by iTRAQ technology using nano LC-MS/MS analysis. As listed in supplementary Table S1, available at *Rheumatology* Online, 1581 proteins were identified. According to the annotation from UniprotKB, 451 proteins (28.5%) are located mainly in the plasma membrane, 503 proteins (31.8%) in the cytoplasm, 238 proteins (15.1%) in the nucleus and the remaining proteins (24.6%) in other subfractions such as the mitochondrion and the endoplasmic reticulum. The expression of ~50% of the proteins increased >2-fold after cold stimulation at 10°C for 3 h (see supplementary Table S1, available at *Rheumatology* Online). The top 30 highly increased proteins are listed in Table 2.

Identification of autoantigens by SERPA in patients with secondary RP

We then used a SERPA approach to screen autoantigens associated with secondary RP. At first, proteins from dHMVEC lysates were separated on two-dimensional gels and were visualized by silver staining (Fig. 2A) or were transferred to membranes for immunoblotting. These membranes were incubated with sera from nine

TABLE 2 List of differentially expressed proteins on the cell surface of dHMVECs after cold stimulation

Accession	Protein name	0.5 h	1 h	3 h
Q96RS6	NudC domain-containing protein 1	3.25	4.24	6.18
P10301	Ras-related protein R-Ras	1.35	3.90	5.95
Q92797	Symplekin	2.94	3.81	5.54
Q643R3	Lysophospholipid acyltranferase LPCAT4	3.06	3.00	5.45
Q99808	Equilibrative nucleoside transporter 1	2.62	3.69	5.21
Q9Y6I9	Testis-expressed sequence 264 protein	2.66	4.11	5.12
Q8TEQ6	Gem-associated protein 5	4.71	6.03	5.08
Q2TAL8	Glutamine-rich protein 1	3.03	4.56	4.99
Q08379	Golgin subfamily A member 2	2.41	4.10	4.74
P49916	DNA ligase 3	2.52	2.94	4.74
P35659	Protein DEK	2.04	3.65	4.67
O60264	SWI/SNF-related matrix-associated actin-dependent regulator of chromatin subfamily A member 5	1.87	4.38	4.52
P60709	Actin, cytoplasmic 1	3.03	3.67	4.28
P55265	Double-stranded RNA-specific adenosine deaminase	2.22	3.86	4.27
Q16643	Drebrin	2.60	3.75	4.24
Q6DD88	Atlastin-3	2.09	3.83	4.14
P29966	Myristoylated alanine-rich C-kinase substrate	1.89	3.61	4.10
Q9ULT8	E3 ubiquitin-protein ligase HECTD1	1.74	3.63	4.08
P61019	Ras-related protein Rab-2A	2.04	3.63	4.03
P61978	hnRNP-K	2.12	3.75	4.03
P01112	GTPase HRas	1.68	2.01	3.95
Q07666	KH domain-containing, RNA-binding, signal transduction-associated protein 1	1.74	3.54	3.92
Q9NZ01	Trans-2,3-enoyl-CoA reductase	1.77	2.08	3.89
Q9NQW6	Actin-binding protein anillin	3.78	5.01	3.86
O00483	NADH dehydrogenase [ubiquinone] 1 alpha subcomplex subunit 4	2.12	2.94	3.86
Q9NP72	Ras-related protein Rab-18	1.96	3.20	3.83
O94901	Protein unc-84 homolog A	2.04	2.77	3.79
P38646	Stress-70 protein, mitochondrial	1.83	3.39	3.76
Q96S97	Myeloid-associated differentiation marker	2.49	3.10	3.75
P49585	Choline-phosphate cytidylyltransferase A	2.68	3.62	3.74

Values are shown as relative expression levels (at 10°C for 0.5, 1 and 3 h) compared with baseline (at 37°C). dHMVECs: dermal human microvascular endothelial cells; hnRNP-K: heterogeneous nuclear ribonucleoprotein K.

patients with RP secondary to SSc (Fig. 2B) or three HCs (Fig. 2C). Six specific spots, which were recognized by sera from >75% of patients, but not by those from HCs, were selected (Fig. 2B). Proteins extracted from the corresponding spots on the silver-stained gel (Fig. 2A) were then subjected to LC-MS/MS analysis and candidate autoantigens were identified by a database search as detailed in Fig. 2D. Among identified candidates, hnRNP-K, a member of the nuclear proteins involved in nucleic acid metabolism [19], was also found in the list of increased proteins on the cell surface under cold stimulation (Table 2), suggesting that hnRNP-K might be a cold-related autoantigen in patients with secondary RP.

Cell surface expression of hnRNP-K under cold stimulation was confirmed by western blot and FACS analysis

The hnRNP proteins are among the most abundant proteins in the nucleus [20]. Indeed, hnRNP-K in dHMVECs under physiological culture conditions was stained intensely in the nucleus by immunofluorescence analysis (see supplementary Fig. S1A and B, available at *Rheumatology* Online). Cold stimulation (10°C for 3 h) induced extranuclear localization of hnRNP-K (see supplementary Fig. S1C and D, available at *Rheumatology* Online), which was nonetheless overwhelmed by intensive staining of nuclear hnRNP-K. To investigate further the appearance of hnRNP-K on the cell surface after cold stimulation, we next performed western blot and FACS analysis. By western blot analysis using concentrated cell surface proteins, hnRNP-K clearly increased in dHMVECs after cold stimulation, but VE-cadherin did not (Fig. 3A). In contrast, the expression level of total hnRNP-K was found to be unchanged during cold stimulation, suggesting that hnRNP-K was not newly synthesized after cold stimulation (Fig. 3A). By FACS analysis, cold-induced expression of hnRNP-K on the cell surface was further confirmed (Fig. 3B). These results collectively suggest that hnRNP-K is a protein that translocates to the cell surface on cold stimulation.

FIG. 2 Identification of autoantigens by SERPA

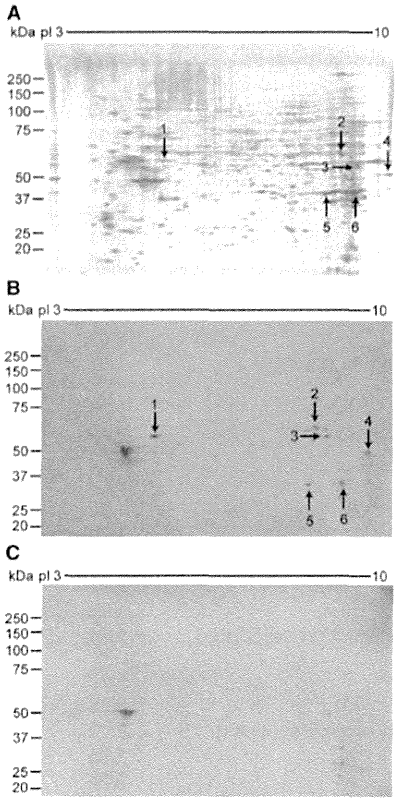

D

no	Access	Identified protein	Mw(kDa)	PI	Coverage(%)
1	P48643	T-complex protein 1 subunit epsilon	59.63	5.66	30.13
	P61978	Heterogeneous nuclear ribonucleoprotein K	50.94	5.54	19.44
	P10809	60 kDa heat shock protein, mitochondrial	61.92	5.87	16.40
	O13283	Ras GTPase-activating protein-binding protein 1	52.13	5.52	18.03
	Q92769	Histone deacetylase 2	55.33	5.91	13.11
	Q9H0R6	Glutamyl-tRNA(Gln) amidotransferase subunit A homolog	57.42	5.68	11.55
	Q05682	Caldesmon	93.19	5.67	3.15
	O15460	Prolyl 4-hydroxylase subunit alpha-2	60.86	5.71	4.11
	Q9UN86	Ras GTPase-activating protein-binding protein 2	54.09	5.55	5.19
2	P29401	Transketolase	67.83	7.66	8.19
	P49748	Very long-chain specific acyl-CoA dehydrogenase, mitochondrial	70.35	8.75	4.27
	Q92804	TATA-binding protein-associated factor 2N	61.79	8.02	7.77
3	P14618	Pyruvate kinase isozymes M1/M2	57.90	7.84	25.05
	P50991	T-complex protein 1 subunit delta	57.89	7.83	11.13
	Q14554	Protein disulfide-isomerase A5	59.56	7.91	11.75
	Q99832	T-complex protein 1 subunit eta	59.33	7.65	11.60
	Q9H078	Caseinolytic peptidase B protein homolog	78.68	9.01	7.64
	P06744	Glucose-6-phosphate isomerase	63.11	8.32	4.30
4	P68104	Elongation factor 1-alpha 1	50.11	9.01	16.45
	P06733	Alpha-enolase	47.14	7.39	9.45
	P55084	Trifunctional enzyme subunit beta, mitochondrial	51.26	9.41	6.12
5	P00338	L-lactate dehydrogenase A chain	36.67	8.27	33.13
	Q14192	Four and a half LIM domains protein 2	32.17	7.55	34.41
	P07355	Annexin A2	38.58	7.75	20.06
	P40926	Malate dehydrogenase, mitochondrial	35.48	8.68	18.05
	P22626	Heterogeneous nuclear ribonucleoproteins A2/B1	37.41	8.95	10.20
	P53597	Succinyl-CoA ligase [GDP-forming] subunit alpha, mitochondrial	36.23	8.79	8.67
	Q16270	Insulin-like growth factor-binding protein 7	29.11	7.90	11.70
6	P04406	Glyceraldehyde-3-phosphate dehydrogenase	36.03	8.46	11.94
	P22626	Heterogeneous nuclear ribonucleoproteins A2/B1	37.41	8.95	10.76
	Q9UKM9	RNA-binding protein Raly	32.44	9.17	8.82
	P23193	Transcription elongation factor A protein 1	33.95	8.38	10.30
	P07355	Annexin A2	38.58	7.75	6.19

(**A**–**C**) Total protein extracts of dHMVECs were separated by two-dimensional PAGE followed by silver staining analysis (**A**) or by western blot analysis with diluted sera from SSc patients with RP (**B**) or from healthy controls (**C**). Arrows and numbers indicate protein spots that were recognized only by the patients' sera. Representative images are shown here. (**D**) List of proteins identified by LC-MS/MS analysis (Mw: molecular weight; pI: isoelectric point). dHMVECs: dermal human microvascular endothelial cells; LC-MS/MS: liquid chromatography–tandem mass spectrometry.

Detection of anti-hnRNP-K antibody in sera from patients with secondary RP by western blot and ELISA analysis

To confirm that hnRNP-K is the autoantigen recognized by sera from patients with secondary RP, full-length recombinant human hnRNP-K protein was prepared and subjected to western blot analysis. As disease controls, SSc patients without RP were intentionally recruited to the study and their sera were investigated. Notably, intense reactivity against recombinant hnRNP-K protein was visualized in sera from SSc patients with RP, but not sera from SSc patients without RP or from HCs (Fig. 3C). This result implies that anti-hnRNP-K antibody is relevant to RP rather than to SSc itself.

We then developed an ELISA system using recombinant hnRNP-K protein to screen anti-hnRNP-K antibody in various CTD patients (SSc, SLE and MCTD) with or without RP and in patients with primary RP (Table 1). As shown in Fig. 3D (top), ELISA analysis revealed that significant elevations of anti-hnRNP-K antibody levels were observed in patients with SSc-, SLE- and MCTD-related RP, but not in patients without RP or those with primary RP compared with HCs (Fig. 3D, top). The prevalence of autoantibodies against hnRNP-K was 26.5% in SSc patients with RP, 42.1% in SLE patients with RP and 40.0% in MCTD patients with RP. In contrast, anti-hnRNP-K positivity was markedly low in CTD patients without RP and was 0% in primary RP patients and HCs (Fig. 3D, top). These results suggest that anti-hnRNP-K antibody is relevant to CTD-related secondary RP rather than to a single CTD.

Of all the CTDs (SSc, SLE and MCTD) in this study, a 30.0% prevalence of anti-hnRNP-K antibody was observed in patients with RP, much higher than that in patients without RP (9.20%, $P = 0.0001$), in patients with primary RP (0%, $P = 0.0314$) or in HCs (0%, $P = 0.0003$) (Fig. 3D, bottom). Anti-hnRNP-K-positive CTD patients had a significantly higher prevalence of RP (88.4%) than

FIG. 3 Cell surface expression of hnRNP-K after cold stimulation and the presence of anti-hnRNP-K autoantibody in sera from patients with secondary RP

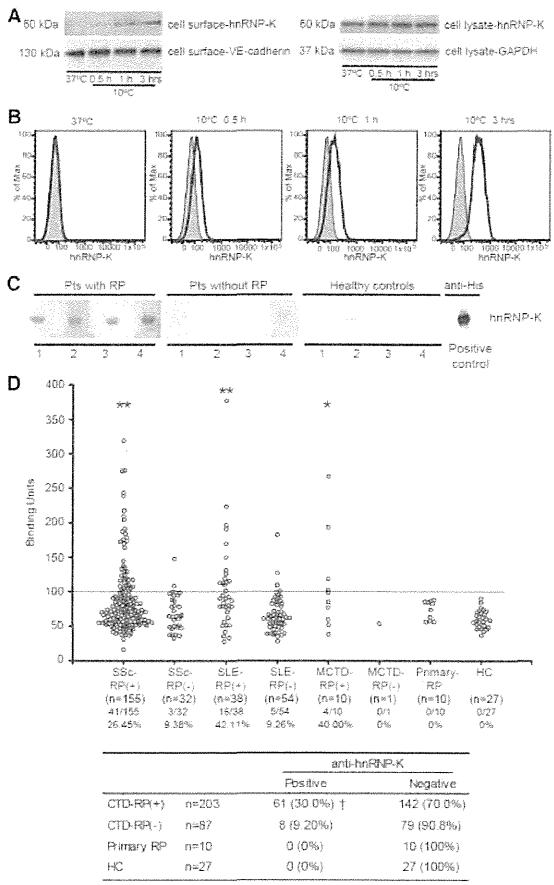

		anti-hnRNP-K	
		Positive	Negative
CTD-RP(+)	n=203	61 (30.0%) †	142 (70.0%)
CTD-RP(-)	n=87	8 (9.20%)	79 (90.8%)
Primary RP	n=10	0 (0%)	10 (100%)
HC	n=27	0 (0%)	27 (100%)

(**A**) Biotinylated surface proteins from dHMVECs incubated at 37°C or 10°C (indicated periods) were precipitated with streptavidin-conjugated agarose beads and analysed by western blot analysis using anti-hnRNP-K. Levels of VE-cadherin surface protein (left panel) and GAPDH expression in total cell lysates (right panel) are shown as controls. (**B**) Cell surface hnRNP-K expression in dHMVECs was analysed by flow cytometry. Shaded histogram indicates staining with control IgG. (**C**) His-tagged recombinant hnRNP-K protein was subjected to western blot analysis using diluted sera from SSc patients with RP, without RP and healthy controls or with anti-6 × His antibody. (**D**) (Top) Serum anti-hnRNP-K antibody levels in indicated CTD patients (with or without RP), primary RP patients and healthy controls were determined by ELISA using recombinant human hnRNP-K. The *y*-axis denotes binding units. The solid horizontal line indicates the positive cut-off limit as described in Materials and methods. Note that this cohort contains a relatively high number of SSc without RP patients and SLE with RP patients, because those patients were intentionally recruited to this study. $^{*}P < 0.05$, $^{**}P < 0.01$ *vs* HCs. (Bottom) Anti-hnRNP-K positivity in patients is summarized. CTD patients are combined here. Values are the number (%) of patients. †$P = 0.00001$ *vs* CTD-RP(−), $P = 0.0314$ *vs* primary RP, $P = 0.0001$ *vs* HCs by Fisher's exact test.
dHMVECs: dermal human microvascular endothelial cells; hnRNP-K: heterogeneous nuclear ribonucleoprotein K; GAPDH: glyceraldehyde-3-phosphate dehydrogenase.

anti-hnRNP-K-negative patients (64.3%, $P = 0.0001$; Table 3). Anti-hnRNP-K antibody showed no correlation with age, gender, smoking or antibodies to U1 ribonucleoprotein (U1-RNP), centromere or SSA/Ro in CTD patients (Table 3). In addition, anti-hnRNP-K showed no correlation with autoantibodies against topoisomerase I (Scl-70) in SSc patients or those against dsDNA or Sm in SLE patients (data not shown). Thus anti-hnRNP-K antibody might be a novel class of biomarker for a subgroup of patients with CTD-related secondary RP.

Discussion

Environmental factors are implicated in the pathogenesis of autoimmune diseases. Previously translocation of intracellular autoantigens to the cell surface was described in ultraviolet radiation-stimulated keratinocytes [21–23]. In the present study, using comprehensive proteomics approaches, we identified hnRNP-K as a novel autoantigen that translocates to the cell surface of dHMVECs after cold stimulation. ELISA analysis revealed that anti-hnRNP-K antibody was significantly elevated in patients with RP secondary to CTDs, but not in patients with primary RP. Thus our data imply hnRNP-K is a putative secondary RP-associated autoantigen that is exposed on the cell surface by cold stimulation.

iTRAQ analysis indicated that cold stimulation in dHMVECs could induce cell surface expression of a variety of proteins, including intracellular proteins, without an overt effect on cell viability, as seen by trypan blue exclusion assay (data not shown). Previous lines of evidence indicate that cytoplasmic and nuclear proteins can reach the cell surface by Golgi-independent non-conventional transport pathways [24–26]. However, it is unknown how cold stimulation induces the translocation of hnRNP-K and other intracellular proteins. Further study is currently under way in our laboratory.

Among many up-regulated proteins identified by iTRAQ analysis, hnRNP-K was the only protein simultaneously identified by SERPA screening. However, our study does not exclude the possibility that there remain other cold-associated autoantigens among these proteins. In particular, since the SERPA approach has limitations in detecting native antigens, antibodies that recognize only native-form autoantigens might have been missed in our study. A screening strategy other than SERPA is necessary to clarify this issue.

hnRNP-K is a 464 amino acid nuclear protein with three K homology domains that mediate DNA and RNA binding [27]. Autoantibodies to hnRNP-K have previously been detected in sera from patients with aplastic anaemia and

TABLE 3 Basic information of 290 patients with CTDs according to the presence of anti-hnRNP-K antibodies

Variable	Positive ($n = 69$)	Negative ($n = 221$)	P value[a]
Age, mean (S.D.), years	52.4 (15.6)	53.3 (15.4)	0.3613
Gender (F:M), *n:n*	61:8	192:29	0.8383
Smoking, % (*n/N*)	18.9 (10/53)	31.6 (56/177)	0.0841
RP, % (*n*)	88.4 (61)	64.3 (142)	0.0001
ANA positivity, % (*n/N*)	94.0 (63/67)	93.1 (203/218)	1.0000
Anti-U1-RNP, % (*n/N*)	26.5 (18/68)	23.1 (50/166)	0.6255
Anti-SSA/Ro positivity, % (*n/N*)	27.9 (19/68)	23.6 (52/220)	0.5202

[a]Univariate analysis using the Mann–Whitney U test or Fisher's exact test. *N*: the number of available patients (varies according to the number of available observations). hnRNP-K: heterogeneous nuclear ribonucleoprotein K.

RA (31% and 24%, respectively), although the co-morbidity of RP in these patients was not described in this report [28]. Autoantibodies to other hnRNPs such as hnRNP-H1 [29], -B1 and -F [30] have also been reported as possible diagnostic markers of CTDs, but their relevance to RP has not been examined.

Although anti-hnRNP-K antibody was identified initially using sera from patients with SSc-related RP, this autoantibody was also detected in sera from RP patients with other CTDs. Notably, anti-hnRNP-K antibody levels in RP patients secondary to SSc, SLE and MCTD were significantly higher than in HCs. In addition, the prevalence of anti-hnRNP-K antibody in SSc patients with RP (26.5%), SLE patients with RP (42.1%) and MCTD patients with RP (40.0%) was markedly higher than in their RP-negative counterparts (9.4%, 9.3% and 0%, respectively) and in primary RP patients (0%). Moreover, anti-hnRNP-K autoantibody was not associated with smoking, which was believed to be a cause of blood vessel narrowing [31], nor with the presence of anti-U1-RNP and ACAs, which are highly related to MCTD and SSc, respectively [32, 33]. Thus these results suggest that anti-hnRNP-K antibody is particularly relevant to CTD-related secondary RP, but not to a single CTD or primary RP. Our findings should be replicated in a larger study.

The pathogenesis of RP likely involves various abnormalities in the vascular, neural and intravascular systems [4]. At present, it remains to be determined whether anti-hnRNP-K autoantibody detected by our ELISA system can bind to hnRNP-K on vascular endothelial cells *in vivo*. In addition, it is unknown whether this autoantibody contributes to the pathogenesis. Because our cohort of patients includes only a limited number of severe RP patients who experienced hospitalization and/or digit loss, it is unknown whether anti-hnRNP-K antibody correlates with the severity of RP. However, it is tempting to speculate that following cold stimulation, anti-hnRNP-K autoantibody may promote antibody-dependent pathogenesis by inducing vascular endothelial damage. As previously reported, anti-endothelial cell antibodies (AECAs) are a heterogeneous group of autoantibodies against various cell surface proteins in endothelial cells and can contribute leucocyte adhesion by inducing adhesion molecules and cytokines in endothelial cells [34–36]. Anti-hnRNP-K antibody may thus be a class of AECA that becomes active under cold stimulation in patients with secondary RP. Further analyses are needed to elucidate the correlation of anti-hnRNP-K autoantibodies with the pathogenesis of secondary RP.

In summary, we provide the first evidence of cold-associated autoantibodies in patients with secondary RP. Anti-hnRNP-K antibody may be a potential biomarker for RP secondary to CTDs. Longitudinal studies are warranted to determine whether the evaluation of anti-hnRNP-K antibody in RP patients may aid in the detection of CTDs in these patients.

Rheumatology key messages

- Cold-associated autoantibody in patients with secondary RP is successfully identified by a proteomic approach.
- hn-RNP-K translocates to the endothelial cell surface upon cold stimulation.
- Anti-hnRNP-K autoantibody may serve as a biomarker for secondary RP.

Acknowledgements

We would like to thank Y. Kanazawa and J. Yamagishi for secretarial assistance and M. Urase and K. Yoshimoto for technical assistance.

Funding: This study was supported by a grant-in-aid for the Program for Promotion of Fundamental Studies in Health Sciences of the National Institute of Biomedical Innovation and a Grant-in-Aid for Research on Biological Markers for New Drug Development (H20-0005) from the Ministry of Health, Labour and Welfare of Japan.

Disclosure statement: The authors have declared no conflicts of interest.

Supplementary data

Supplementary data are available at *Rheumatology* Online.

References

1 Unwin RD, Griffiths JR, Whetton AD. Simultaneous analysis of relative protein expression levels across multiple samples using iTRAQ isobaric tags with 2D nano LC-MS/MS. Nat Protoc 2010;5:1574–82.

2 Serada S, Fujimoto M, Ogata A *et al*. iTRAQ-based proteomic identification of leucine-rich alpha-2 glycoprotein as a novel inflammatory biomarker in autoimmune diseases. Ann Rheum Dis 2010;69:770–4.

3 Yokoyama T, Enomoto T, Serada S *et al*. Plasma membrane proteomics identifies bone marrow stromal antigen 2 as a potential therapeutic target in endometrial cancer. Int J Cancer 2013;132:472–84.

4 Herrick AL. The pathogenesis, diagnosis and treatment of Raynaud phenomenon. Nat Rev Rheumatol 2012;8:469–79.

5 Bakst R, Merola JF, Franks AG Jr, Sanchez M. Raynaud's phenomenon: pathogenesis and management. J Am Acad Dermatol 2008;59:633–53.

6 Dimant J, Ginzler E, Schlesinger M *et al*. The clinical significance of Raynaud's phenomenon in systemic lupus erythematosus. Arthritis Rheum 1979;22:815–9.

7 Grader-Beck T, Wigley FM. Raynaud's phenomenon in mixed connective tissue disease. Rheum Dis Clin North Am 2005;31:465–81, vi.

8 Maricq HR, Harper FE, Khan MM, Tan EM, LeRoy EC. Microvascular abnormalities as possible predictors of disease subsets in Raynaud phenomenon and early connective tissue disease. Clin Exp Rheumatol 1983;1:195–205.

9 Srivastava R, Aslam M, Kalluri SR *et al*. Potassium channel KIR4.1 as an immune target in multiple sclerosis. N Engl J Med 2012;367:115–23.

10 Serada S, Fujimoto M, Takahashi T *et al*. Proteomic analysis of autoantigens associated with systemic lupus erythematosus: anti-aldolase A antibody as a potential marker of lupus nephritis. Proteomics Clin Appl 2007;1:185–91.

11 He P, Naka T, Serada S *et al*. Proteomics-based identification of alpha-enolase as a tumor antigen in non-small lung cancer. Cancer Sci 2007;98:1234–40.

12 Masi AT. Preliminary criteria for the classification of systemic sclerosis (scleroderma). Subcommittee for scleroderma criteria of the American Rheumatism Association Diagnostic and Therapeutic Criteria Committee. Arthritis Rheum 1980;23:581–90.

13 Tan EM, Cohen AS, Fries JF *et al*. The 1982 revised criteria for the classification of systemic lupus erythematosus. Arthritis Rheum 1982;25:1271–7.

14 Hochberg MC. Updating the American College of Rheumatology revised criteria for the classification of systemic lupus erythematosus. Arthritis Rheum 1997;40:1725.

15 Kasukawa R, Tojo T, Miyawaki S. Preliminary diagnostic criteria for classification of mixed connective tissue disease. In: Kasukawa R, Sharp GC, eds. Mixed Connective Tissue Diseases and Antinuclear Antibodies. Amsterdam, the Netherlands: Elsevier, 1987:41–7.

16 Brennan P, Silman A, Black C *et al*. Validity and reliability of three methods used in the diagnosis of Raynaud's phenomenon. The UK Scleroderma Study Group. Br J Rheumatol 1993;32:357–61.

17 Umegaki-Arao N, Tamai K, Nimura K *et al*. Karyopherin alpha2 is essential for rRNA transcription and protein synthesis in proliferative keratinocytes. PLoS One 2013;8:e76416.

18 Yang L, Serada S, Fujimoto M *et al*. Periostin facilitates skin sclerosis via PI3K/Akt dependent mechanism in a mouse model of scleroderma. PLoS One 2012;7:e41994.

19 Han SP, Tang YH, Smith R. Functional diversity of the hnRNPs: past, present and perspectives. Biochem J 2010;430:379–92.

20 Dreyfuss G, Matunis MJ, Pinol-Roma S, Burd CG. hnRNP proteins and the biogenesis of mRNA. Annu Rev Biochem 1993;62:289–321.

21 Furukawa F, Kashihara-Sawami M, Lyons MB, Norris DA. Binding of antibodies to the extractable nuclear antigens SS-A/Ro and SS-B/La is induced on the surface of human keratinocytes by ultraviolet light (UVL): implications for the pathogenesis of photosensitive cutaneous lupus. J Invest Dermatol 1990;94:77–85.

22 Wang B, Dong X, Yuan Z, Zuo Y, Wang J. SSA/Ro antigen expressed on membrane of UVB-induced apoptotic keratinocytes is pathogenic but not detectable in supernatant of cell culture. Chin Med J 1999;112:512–5.

23 Golan TD, Elkon KB, Gharavi AE, Krueger JG. Enhanced membrane binding of autoantibodies to cultured keratinocytes of systemic lupus erythematosus patients after ultraviolet B/ultraviolet A irradiation. J Clin Invest 1992;90:1067–76.

24 Nickel W, Seedorf M. Unconventional mechanisms of protein transport to the cell surface of eukaryotic cells. Annu Rev Cell Dev Biol 2008;24:287–308.

25 Nickel W, Rabouille C. Mechanisms of regulated unconventional protein secretion. Nat Rev Mol Cell Biol 2009;10:148–55.

26 Nickel W. Pathways of unconventional protein secretion. Curr Opin Biotechnol 2010;21:621–6.

27 Bomsztyk K, Denisenko O, Ostrowski J. hnRNP K: one protein multiple processes. Bioessays 2004;26:629–38.

28 Qi Z, Takamatsu H, Espinoza JL *et al*. Autoantibodies specific to hnRNP K: a new diagnostic marker for immune pathophysiology in aplastic anemia. Ann Hematol 2010;89:1255–63.

29 Van den Bergh K, Hooijkaas H, Blockmans D *et al*. Heterogeneous nuclear ribonucleoprotein h1, a novel nuclear autoantigen. Clin Chem 2009;55:946–54.

30 Op De Beeck K, Maes L, Van den Bergh K *et al*. Heterogeneous nuclear RNPs as targets of autoantibodies in systemic rheumatic diseases. Arthritis Rheum 2012;64:213–21.

31 D.S.G. Tobacco report: PHS Study Group, after 14-month survey, agrees that smoking is indeed harmful. Science 1964;143:227.

32 Buchanan RR, Riglar AG. The titre of anti-centromere antibodies: its relationship to Raynaud's phenomenon and vascular occlusion. Br J Rheumatol 1989;28:221–6.

33 Furtado RN, Pucinelli ML, Cristo VV, Andrade LE, Sato EI. Scleroderma-like nailfold capillaroscopic abnormalities are associated with anti-U1-RNP antibodies and Raynaud's phenomenon in SLE patients. Lupus 2002;11: 35–41.

34 Carvalho D, Savage CO, Black CM, Pearson JD. IgG antiendothelial cell autoantibodies from scleroderma patients induce leukocyte adhesion to human vascular endothelial cells in vitro. Induction of adhesion molecule expression and involvement of endothelium-derived cytokines. J Clin Invest 1996;97:111–9.

35 Del Papa N, Guidali L, Sironi M *et al.* Anti-endothelial cell IgG antibodies from patients with Wegener's granulomatosis bind to human endothelial cells in vitro and induce adhesion molecule expression and cytokine secretion. Arthritis Rheum 1996;39:758–66.

36 Lin CF, Chiu SC, Hsiao YL *et al.* Expression of cytokine, chemokine, and adhesion molecules during endothelial cell activation induced by antibodies against dengue virus nonstructural protein 1. J Immunol 2005;174:395–403.

Annexin A4 induces platinum resistance in a chloride-and calcium-dependent manner

Akiko Morimoto[1,2], Satoshi Serada[2], Takayuki Enomoto[3], Ayako Kim[2], Shinya Matsuzaki[1] ,Tsuyoshi Takahashi[2,4] ,Yutaka Ueda[1], Kiyoshi Yoshino[1], Masami Fujita[1], Minoru Fujimoto[2], Tadashi Kimura[1] and Tetsuji Naka[2]

[1] Department of Obstetrics and Gynecology, Osaka University Graduate School of Medicine, Japan

[2] Laboratory for Immune Signals, National Institute of Biomedical Innovation, Japan

[3] Department of Obstetrics and Gynecology, Niigata University Medical School, Japan

[4] Department of Surgery, Osaka University Graduate School of Medicine, Japan

Correspondence to: *Tetsuji Naka* , ***email:*** *tnaka@nibio.go.jp*

Keywords: Annexin A4; platinum resistance; annexin repeat; chloride ion

Received: *April 04, 2014* ***Accepted:*** *August 03, 2014* ***Published:*** *August 04, 2014*

ABSTRACT

Platinum resistance has long been a major issue in the treatment of various cancers. We previously reported that enhanced annexin A4 (ANXA4) expression, a Ca^{2+}-regulated phospholipid-binding protein, induces chemoresistance to platinum-based drugs. In this study, we investigated the role of annexin repeats, a conserved structure of all the annexin family, responsible for platinum-resistance as well as the effect of knockdown of ANXA4. ANXA4 knockdown increased sensitivity to platinum-based drugs both *in vitro* and *in vivo*. To identify the domain responsible for chemoresistance, ANXA4 deletion mutants were constructed by deleting annexin repeats one by one from the C terminus. Platinum resistance was induced both *in vitro* and *in vivo* in cells expressing either full-length ANXA4 or the deletion mutants, containing at least one intact annexin repeat. However, cells expressing the mutant without any calcium-binding sites in the annexin repeated sequence, which is essential for ANXA4 translocation from the cytosol to plasma membrane, failed to acquire platinum resistance. After cisplatin treatment, the intracellular chloride ion concentration, whose channel is partly regulated by ANXA4, significantly increased in the platinum-resistant cells. These findings indicate that the calcium-binding site in the annexin repeat induces chemoresistance to the platinum-based drug by elevating the intracellular chloride concentration.

INTRODUCTION

Since cisplatin was first introduced as an anticancer drug in the 1970s [1], various platinum-based drugs have been developed and widely used not only against gynecological but also against other cancers, including lung, colorectal, testicular, prostate and bladder cancer [2-6]. Although these platinum-based drugs have significantly contributed to improve survival rates, chemoresistance to these drugs has become a major problem in recent years [7-9]. It has now been elucidated that the mechanism of platinum resistance is mediated by reduced platinum accumulation, increased platinum detoxification, increased repair of platinum–DNA adducts and inhibited apoptosis [10-12]. Several proteins have been reported to be candidate factors such as copper transporters: CTR1[13], ATP7A and ATP7B[14-17]; multidrug resistance protein 2 (MRP2) [18-20]; glutathione S-transferase enzyme π (GSTπ) [21]; excision cross-complementing gene 1 (ERCC1) [22]; receptor-interacting protein 1 (RIP1) [23]; microRNAs [24-26]; and p53 [27]. In contrast, there are still several proteins related to platinum resistance without a full understanding of how these proteins help cells to confer platinum-based drugs.

We recently reported that annexin A4 (ANXA4) is overexpressed in ovarian clear cell carcinoma and

induces chemoresistance to platinum-based drugs [28]. Annexins are calcium-regulated and negatively charged phospholipid membrane-binding proteins. The basic structure of annexins consists of 2 major domains: a conserved structural element called an annexin repeat, a segment of 70 amino acid residues at the C terminus, and the N-terminal region unique for a given member of the family and determining individual annexin properties *in vivo*. The annexin repeat possesses the calcium and membrane binding sites and is responsible for mediating the canonical membrane binding properties [29]. These domains in ANXA4 are surrounded by relatively short amino and carboxy termini that do not have any known function [30]. ANXA4 is involved in membrane permeability, exocytosis and regulation of chloride channels in a calcium-dependent manner [29, 31-33]. ANXA4 is almost exclusively expressed in epithelial cells [34]. With regard to cancer, ANXA4 overexpression has been reported in various tumours, such as lung, gastric, colorectal, renal, pancreatic, ovarian and prostate cancer [28, 35-39] and is associated with tumour invasiveness, metastasis and chemoresistance [37, 40]. Moreover, ANXA4 has been shown to be associated with resistance to platinum-based drugs [28, 41-43].

ANXA4-induced platinum resistance appears to be mediated in part by the increased extracellular efflux of platinum mediated by the copper transporter ATP7A[28, 44]. Another mechanism of ANXA4-induced chemoresistance is the modulation of NF-κB transcriptional activity [45]. ANXA4 suppresses NF-κB transcriptional activity through interaction with the p50 subunit in a calcium-dependent manner; ANXA4 causes resistance to apoptosis induction by etoposide.

While ANXA4 prominently associated with chemoresistance, the functional domain of ANXA4 remains unclear. Therefore, to clarify the functional domain of ANXA4 is required to understand detailed mechanisms of the chemoresistance induced by ANXA4 and also overcome chemoresistance. In this study, focusing on platinum resistance, we aimed to identify the ANXA4 domain relevant to chemoresistance with regard to its structure as well as to test whether knockdown of ANXA4 expression could improve platinum resistance. Our data showed that the annexin repeat plays an important role in platinum resistance induced by ANXA4, which occurs in a calcium-dependent manner.

RESULTS

Establishment of ANXA4 knockdown RMG-I cells

To create cell lines with a stable ANXA4 knockdown, we analysed ANXA4 expression in ovarian cancer cells using western blotting. ANXA4 expression was strong in clear cell carcinoma cell lines (OVTOKO, OVISE and RMG-I) compared with serous adenocarcinoma cell lines (A2780, OVCAR3 and OVSAHO) and a mucinous adenocarcinoma cell line (MCAS; Fig. 1A). To see whether blocking ANXA4 expression was a valid chemosensitising strategy for ovarian clear cell carcinoma treatment, ANXA4 was stably suppressed using an ANXA4 shRNA plasmid. We established RMG-I-Y4 and R5 cell clones as well as RMG-I NC7 cell clones transfected with the empty vector as a control. Compared with RMG-I NC7 and untransfected control parent RMG-I cells, ANXA4 expression was markedly down-regulated at the protein level in RMG-I-Y4 and RMG-I-R5 cells (Fig. 1B). In the absence of any drug treatment, the growth rate among the 4 cell lines was similar *in vitro* (data not shown).

Knockdown of ANXA4 expression enhances sensitivity to cisplatin and carboplatin

The sensitivity to cisplatin and carboplatin was assessed in the 3 RMG-I clones NC7, R5 and Y4. Compared with the IC_{50} for cisplatin in NC7 cells, IC_{50} was significantly decreased in Y4 cells and R5 cells ($p < 0.01$; Fig. 1C, left panel). Similarly, IC_{50} for carboplatin significantly decreased in Y4 cells and R5 cells compared with NC7 cells ($p < 0.01$; Fig. 1C, right panel). IC_{50} for cisplatin and carboplatin decreased approximately 2-fold because of the knockdown of ANXA4 expression.

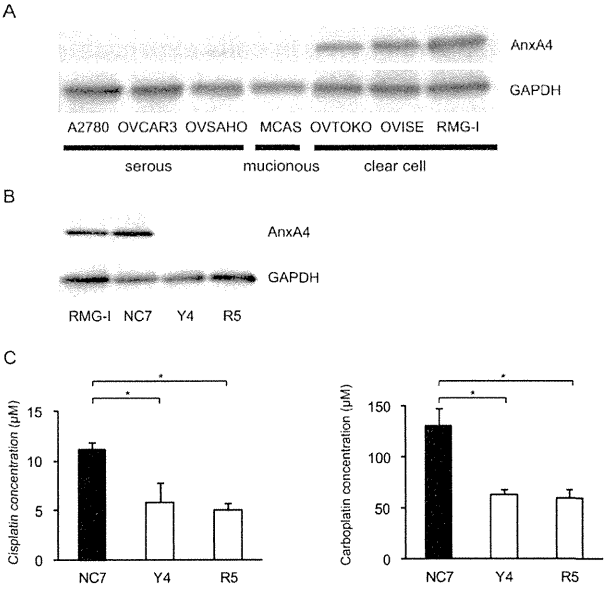

Fig.1: Knockdown of ANXA4 expression attenuates platinum resistance. (A) ANXA4 expression in indicated ovarian cancer cell lines and (B) established ANXA4 knockdown RMG-I cells (R5 and Y4) was confirmed using Western blotting. (C) IC_{50} for both cisplatin and carboplatin was significantly reduced in R5 and Y4 cells compared with NC7 cells. Data are presented as mean ± SD (*$p < 0.01$).